

JAMES | Journal of Advances in Modeling Earth Systems*



RESEARCH ARTICLE

10.1029/2022MS003572

Key Points:

- We implement a numerical version of a multiple-scale Quasi-Geostrophic (MSQG) model
- Multiple Scale Quasi Geostrophy allows for variable stratification and variable Coriolis parameter
- The MSQG model reproduces the dynamics of a high resolution primitive equation model

Correspondence to:

B. Deremble, bruno.deremble@cnrs.fr

Citation:

Deremble, B., Uchida, T., Dewar, W. K., & Samelson, R. M. (2023). Eddy-mean flow interaction with a multiple scale quasi geostrophic model. *Journal of Advances in Modeling Earth Systems*, 15, e2022MS003572. https://doi.org/10.1029/2022MS003572

Received 16 FEB 2023 Accepted 11 SEP 2023

Author Contributions:

Conceptualization: Bruno Deremble, Takaya Uchida, William K. Dewar, Roger M. Samelson

Data curation: Bruno Deremble **Formal analysis:** Bruno Deremble, William K. Dewar

Funding acquisition: William K. Dewar Investigation: Bruno Deremble, Takaya Llebida

Methodology: Bruno Deremble, William K. Dewar, Roger M. Samelson Resources: Bruno Deremble, Roger M. Samelson

Software: Bruno Deremble Validation: Bruno Deremble Writing – original draft: Bruno Deremble

© 2023 The Authors. Journal of Advances in Modeling Earth Systems published by Wiley Periodicals LLC on behalf of American Geophysical Union. This is an open access article under the terms of the Creative Commons Attribution-NonCommercial License, which permits use, distribution and reproduction in any medium, provided the original work is properly cited and is not used for commercial purposes.

Eddy-Mean Flow Interaction With a Multiple Scale Quasi Geostrophic Model

Bruno Deremble¹, Takaya Uchida^{1,2}, William K. Dewar^{1,3}, and Roger M. Samelson⁴

¹Institut des Géosciences de l'Environnement, CNRS, INRAE, IRD, Grenoble-INP, Université Grenoble Alpes, Grenoble, France, ²Center for Ocean Atmospheric Prediction Studies, Florida State University, Tallahassee, FL, USA, ³Department of Earth, Ocean, and Atmospheric Science, Florida State University, Tallahassee, FL, USA, ⁴College of Earth, Ocean, and Atmospheric Sciences, Oregon State University, Corvallis, OR, USA

Abstract Parameterization of mesoscale eddies in coarse resolution ocean models is necessary to include the effect of eddies on the large-scale oceanic circulation. We propose to use a multiple-scale Quasi-Geostrophic (MSQG) model to capture the eddy dynamics that develop in response to a prescribed large-scale flow. The MSQG model consists in extending the traditional quasi geostrophic (QG) dynamics to include the effects of a variable Coriolis parameter and variable background stratification. Solutions to this MSQG equation are computed numerically and compared to a full primitive equation model. The large-scale flow field permits baroclinically unstable QG waves to grow. These instabilities saturate due to non-linearities and a filtering method is applied to remove large-scale structures that develop due to the upscale cascade. The resulting eddy field represents a dynamically consistent response to the prescribed background flow, and can be used to rectify the large-scale dynamics. Comparisons between Gent-McWilliams eddy parameterization and the present solutions show large regions of agreement, while also indicating areas where the eddies feed back onto the large scale in a manner that the Gent-McWilliams parameterization cannot capture. Also of interest is the time variability of the eddy feedback which can be used to build stochastic eddy parameterizations.

Plain Language Summary Climate models are running at horizontal spatial resolutions that capture only the basin-scale dynamics. This is a strong limitation because the missing mesoscale eddies have a non-negligible impact on the large-scale flow. The problem of including the effect of eddies in climate models is a long standing issue in the ocean modeling community. In this work, we decompose the ocean dynamics into stationary large-scale dynamics and turbulent small-scale dynamics. One can thus write a system of equations for the large-scale dynamics—which can be interpreted as the ocean dynamics given by climate models—and another system of equations for the small-scale dynamics. The numerical implementation of this model reveals that this reduced system of equations faithfully reproduces the dynamics of a high resolution ocean model. This paper is a first step that will eventually guide us to use this model as a parameterization of unresolved scales in low resolution ocean models.

1. Introduction

Parameterization of mesoscale eddies in coarse resolution models is a long standing issue in oceanography because while eddies have a disproportionately large impact on the global transport of heat and tracers (Gnanadesikan et al., 2015; Griffies et al., 2015), we often lack the computational resources to accurately resolve them. As of today, it is still not clear how small-scale eddies affect the large-scale oceanic circulation nor how their effects should be parameterized.

Gent and McWilliams (1990, henceforth denoted GM) accomplished a major breakthrough to build such a parameterization when they proposed a first order closure scheme that mimics the role of the eddies based on the large-scale stratification only. This parameterization has been discussed and enhanced (Griffies, 1998; McDougall & McIntosh, 2001; Meunier et al., 2023), and is now routinely used in ocean models (Gent, 2011). The idea behind this parameterization is that ocean eddies restore slanted isopycnal surfaces to a level state of rest in an adiabatic way. In terms of energy transfer, this corresponds to a situation where eddies tap into the large-scale potential energy reservoir and have thus a tendency to flatten isopycnal surfaces.

Since the seminal work of Gent and McWilliams (1990), there have been several attempts to augment the formulation of the parameterization of mesoscale eddies. For instance, Treguier et al. (1997) and Visbeck et al. (1997)

DEREMBLE ET AL. 1 of 25



Journal of Advances in Modeling Earth Systems

10.1029/2022MS003572

Writing – review & editing: Takaya Uchida, William K. Dewar, Roger M Samelson have proposed to adjust the magnitude of the rectification based on a stability criteria of the large-scale flow. Cessi (2008) and Eden and Greatbatch (2008), on the other hand, try to constrain the rectification based on the eddy energetics. It is also a well know issue that the rectification is sensitive to how the adiabaticity is relaxed near the surface and bottom boundaries (e.g., Ferrari et al., 2008, 2010; Uchida, 2019, his Appendix D). A synthesis of the different approaches appears in Gent (2011) and references therein. More recently D. P. Marshall et al. (2012) have proposed a GEOMETRIC approach for which the amplitude of the rectification scales with the eddy geometry and energy—dynamical variables that characterize the unresolved eddy activity—and has shown some success (Mak et al., 2017, 2022). Inspired by all these developments, we propose the hypothesis that there exists an alternative to the GM parameterization in the form of a dynamical model of intermediate complexity. To test this hypothesis, we will use a modified version of the multiple scale quasi geostrophic (MSQG) model originally derived by Pedlosky (1984) and confirmed and expanded by Grooms et al. (2011). The derivation of the original multiple scale model relies on the principle of scale separation between the large-scale dynamics and the small-scale turbulent flow. With this separation of scales, one can decompose the Navier-Stokes equations into two sets of equations: an equation set for the large-scale Planetary geostrophic (PG) dynamics and one equation set for the small-scale Quasi-Geostrophic (QG) dynamics. The QG model derived in this framework of multiple scale formalism is richer than the traditional OG equations because the background stratification and the Coriolis parameters are functions of space (and thus, the deformation radius is no longer restricted to be spatially uniform; Theiss, 2006). Eddies generated in this framework will then feel the slow variations of the large-scale structure of the thermocline. Killworth and Blundell (2007), Smith (2007), and Tulloch et al. (2011) have worked on the linear version of this model in a realistic context: they computed the characteristic length scales and time scales of the baroclinic instability and showed that there is a good agreement between the observed eddy length scale and the instability length scale. Following the same idea, Venaille et al. (2011) proposed a non-linear implementation of this multiple scale model: from an ocean general circulation model they extracted vertical hydrographic and velocity profiles in several locations in the Antarctic circumpolar current (ACC) and used these profiles to force several doubly periodic QG models at all these locations. They showed that each QG model is capable of reproducing some oceanic structures such as rings or jets and they found a good correspondence between the structure of the flow in each OG module and in a primitive equation (PE) simulation; although with an offset in the energy levels.

Our implementation of the MSQG model departs from the original derivation because we add a damping term in the equation of evolution of potential vorticity (PV). We will actually show that this damping term can be interpreted as a coupling between the large-scale and small-scale components of the dynamics, a point that is absent in Pedlosky's derivation. Moreover we will deploy the MSOG equation at the basin scale: we will handle as best as we can the translation of a well posed mathematical multiple-scale framework in a numerical model. To our knowledge, this is the first time such a model is implemented at the basin scale. In order to validate the model, we will first construct a reference high resolution PE configuration of an extra-tropical ocean basin. In this configuration, we will diagnose the mean flow and eddy dynamics. This run will serve as a reference configuration. We will then run the MSOG model with the background flow of the reference run; we will then compare the eddy statistics of the full model and the reduced model. For a given mean flow, we will study how the eddies organize to feedback onto the large-scale solution. The study of the eddy-mean flow interaction with a stationary mean flow is clearly the first step toward a more advanced setup where the MSQG model would run in real time alongside a coarse resolution PE model in a form of superparameterization. We will not tackle this latter point in this article but as a motivation, we state that this superparameterization approach is richer than the GM parameterization for at least three reasons. First, the GM parameterization is meant to flatten isopyenal surfaces everywhere (no matter the type of oceanic dynamics). This property is based on the dynamics we expect from baroclinic instability and is probably a very good approximation in most places of the ocean. However, we know that eddies have sometimes the tendency to steepen isopycnal slopes, especially near jets (Porta Mana & Zanna, 2014; Shevchenko & Berloff, 2015; Waterman & Jayne, 2011). In such places, first order parameterizations may misrepresent ocean dynamics. Another reason is that by design, first order closures use a locality hypothesis: eddies are generated and interact with the mean flow at the same location. However, with the MSQG model, eddies are explicitly represented and they are free to propagate in and out of regions of high and low baroclinicity. Thus, we expect that the inverse cascade (IC) will be effective beyond the local region of eddy production. And the last reason is that first order closures predict a stationary response for a given mean flow. The community has been aware of this issue for several years and there have been several propositions to build a non stationary rectification of the large-scale flow mostly in the form of energy backscattering where

DEREMBLE ET AL. 2 of 25

one reinjects the sub-grid (unresolved) energy back into the resolved flow as eddies would rectify the large-scale flow if resolved (e.g., Bachman, 2019; Jansen et al., 2019; Juricke et al., 2019; Uchida et al., 2022, and references therein) and/or stochastic parameterizations (Grooms, 2016; Guillaumin & Zanna, 2021; Li et al., 2023; Mémin, 2014; Porta Mana & Zanna, 2014; Ryzhov et al., 2020). Our approach provides a natural way to handle this issue of non-stationary response and we will see how our implementation can actually be used to guide stochastic parameterizations.

The plan of the paper is as follows. In Section 2, we describe the MSQG equation and we discuss the link between the IC in QG and the GM parameterization. In Section 3, we set up a high resolution PE model that will serve as a reference case. In this section, we also compare the dynamics of the MSQG model when forced by the mean flow of the eddy resolving model. In Section 4, we analyze how eddies modify the large-scale PV, and the large-scale buoyancy. We also discuss how these results can be used as a substitute to the GM parameterization.

2. Model and Methods

2.1. Primitive Equations in the General Case

The generic hydrostatic Boussinesq primitive equations in the oceanic context are

$$\frac{\partial \boldsymbol{u}_h}{\partial t} + \boldsymbol{u} \cdot \nabla \boldsymbol{u}_h + f \boldsymbol{k} \times \boldsymbol{u}_h = -\nabla_h P + \mathcal{T} + D_u$$
 (1a)

$$\frac{\partial \tilde{b}}{\partial t} + \tilde{\boldsymbol{u}} \cdot \nabla \tilde{b} = Q + D_b + \tilde{\mathcal{R}}$$
 (1b)

$$\frac{\partial P}{\partial z} = b \tag{1c}$$

$$\nabla \cdot \boldsymbol{u} = 0, \tag{1d}$$

with the buoyancy \underline{b} , the velocity \underline{u} (and the subscript h is for the horizontal component). Note that we write all PE variables with a tilde $(\underline{u}, \underline{b})$ to not confuse these variables with the QG variables that we will introduce soon. P is the dynamical pressure (pressure divided by a constant density in the Boussinesq framework), f the Coriolis parameter and k is the unit vertical vector. T is the wind stress forcing at the surface only and D_u is a dissipative term: bi-harmonic viscosity plus linear bottom friction (BF) for the velocity field just above the sea floor. For simplicity we use a linear equation of state

$$b = g\alpha\theta, \tag{2}$$

with θ the potential temperature, α the thermal expansion coefficient, and g the acceleration due to gravity. In the rhs of Equation 1b we have, a forcing term Q which will be a relaxation toward a prescribed temperature profile (to mimic the combination of solar heat flux and air-sea heat fluxes with no seasonal variations). In the buoyancy equation, there is also a dissipation term $D_b = -A_4 \nabla^4 \underline{b} + A_z \partial^2 \underline{b}/\partial z^2$; with A_4 , and A_z the constant horizontal and vertical diffusivity coefficients respectively.

The last term in Equation 1b, $\stackrel{\mathcal{R}}{\sim}$ corresponds to the effect of small-scale eddies on the large-scale flow which is traditionally included only in coarse resolution models. We recall the main properties of this term in the next subsection. We also introduce the Reynolds decomposition

$$X = \overline{X} + X'. \tag{3}$$

with the overbar the ensemble averaging operator and X' the deviation from the mean. Because in this study we will use a stationary forcing, we can reinterpret the ensemble averaging as a time averaging. Also, we use "large-scale flow," "mean flow," or background flow to designate the ensemble mean. And we use "small-scale flow" or "eddy flow" to designate the deviation with respect to the mean.

DEREMBLE ET AL. 3 of 25

2.2. Quasi Geostrophic Model for the Eddy Flow

To model the evolution of the eddy flow, we deploy a MSQG model. In the multiple scale formalism originally derived by Pedlosky (1984) (see also Grooms et al., 2011; Jamet et al., 2021), the small-scale dynamics are governed by the QG equation which is forced solely by the large-scale flow. The traditional QG equations with only one dynamical variable is known to faithfully reproduce mesoscale eddies with a small number of levels in the vertical discretization. The QG model is thus a good candidate for a model of intermediate complexity (compared to the PE model) that still exhibits realistic eddy dynamics. In this system of equation, the main variable is the QG PV

$$q = \nabla^2 \psi + \Gamma \psi, \tag{4}$$

with ψ the small-scale stream function and Γ is the vertical stretching operator

$$\Gamma \psi = \frac{\partial}{\partial z} \left(\frac{f^2}{N^2} \frac{\partial \psi}{\partial z} \right) = \frac{\partial}{\partial z} \frac{f}{N^2} b, \tag{5}$$

with

$$b = f \frac{\partial \psi}{\partial z},\tag{6}$$

the small-scale buoyancy, and

$$N^2 = \frac{\partial B}{\partial z},\tag{7}$$

the Brunt-Vaisala frequency squared; *B* being the prescribed background buoyancy. Note that in order not to confuse the background variables (which are prescribed) and the averaged variables of the eddy flow (noted with an overbar), we write all background variables with a capital letter.

The QG model is posed theoretically in the continuously stratified setting, for consistency with the primitive-equation formulation, but only a small number of levels, or equivalent local vertical modes, are required to represent the dominant mesoscale eddy fluxes, because of the small length scales of the higher modes. This vertically-discretized QG model can be physically interpreted as an equivalent layer model (see Section 3.2 and Appendix B). The numerical implementation nonetheless uses a 3D elliptic solver with $\psi = 0$ on the lateral boundaries (no-normal-flow), and $\partial \psi/\partial z = 0$ at the upper and lower boundaries (zero buoyancy anomaly), which gives a 3D solution for ψ that is consistent with the layer-model interpretation. Note that the top and bottom boundary conditions correspond to the standard assumption in QG that buoyancy vanishes at the top and bottom surfaces. As we shall see henceforth, this condition is very helpful in the context of eddy parameterization (see discussion in the next section). In the general case, it is of course possible to adopt a "surface QG" boundary condition where the top and bottom buoyancy become a dynamical variable (a strategy that we did not adopt here; see e.g., Roullet et al., 2012).

The key point of the MSQG model is that the Coriolis parameter and the background buoyancy frequency can both vary slowly in space (Pedlosky, 1984). This is actually a major difference compared to the traditional definition of QG PV where f and N^2 are constants in the stretching operator (Vallis, 2017). Although richer than traditional QG, we anticipate that with such Wentzel–Kramers–Brillouin assumption that f and N^2 are slow functions of space, the MSQG model will not conserve energy and enstrophy (see Appendix B). The equation of evolution of QG PV is

$$\frac{\partial q}{\partial t} + \boldsymbol{u} \cdot \nabla q + \boldsymbol{U} \cdot \nabla q + \boldsymbol{u} \cdot \overline{\nabla} Q = \mathcal{D}_q - \mathcal{F}_q, \tag{8}$$

with u the small-scale velocity field

$$\mathbf{u} = \left(-\frac{\partial \psi}{\partial y}, \frac{\partial \psi}{\partial x}\right). \tag{9}$$

and with U the rotational component of the background flow

DEREMBLE ET AL. 4 of 25

with Ψ the background stream function. In the multiple scale QG formalism, the background PV is

$$O = f + \Gamma \Psi, \tag{11}$$

and the gradient of the large-scale vorticity is

$$\overline{\nabla}O = (\Gamma V. \beta - \Gamma U). \tag{12}$$

where the operator $\overline{\nabla}$ is written with an overbar to emphasize the multiple scale formalism (see Appendix B). The dissipative effects and BF are written as

$$\mathcal{D}_q = A_2 \nabla^2 q - A_4 \nabla^4 q - r \nabla^2 \psi, \tag{13}$$

with A_2 and A_4 the harmonic and bi-harmonic dissipation coefficients, and r the BF coefficient (non zero at the bottom only). The harmonic and bi-harmonic operators act on the total PV: in the PE, that would correspond to the combined effect of a viscous operator acting on the velocity field and a diffusivity operator on the buoyancy with the same viscous and diffusivity coefficients. Last, \mathcal{F}_a is a filtering term to ensure that q remains a small-scale variable. It is in fact a parameterization of the term $\nabla \cdot ua$ which formally appears in the derivation as a higher order term in the multiple-scale expansion (Grooms et al., 2011). In a similar context, Uchida et al. (2022) parameterized this term as a damping of the large-scale component of q:

$$\mathcal{F}_q = \frac{\hat{q}}{\tau_\ell},\tag{14}$$

where τ_f is the low pass filtered PV and τ_f a relaxation time scale (which should be a fast time scale compared to the ventilated thermocline time scale; see also A1 in Appendix A). We implemented this model with the basilisk framework (http://basilisk.fr). It is freely available (see Data Availability Statement Section) and we provide more details on the numerical recipes in Appendix B.

2.3. GM Parameterization

We now turn our attention to the strategy to couple a low resolution implementation of Equation 1 with a high resolution MSQG model. The term \mathcal{R} in Equation 1b represents the effect of the small-scale eddies on the large-scale flow and is usually active only for coarse resolution models. Formally this term is meant to represent the unresolved eddy-eddy interaction: from a straightforward Reynolds decomposition, one gets

$$\mathcal{R} = -\nabla \cdot \overline{\boldsymbol{u}'b'},\tag{15}$$

We decompose the eddy flux $\overline{\underline{u'b'}}$ into a diapycnal and an isopycnal flux and neglect the diapycnal flux (to mimic the effect of baroclinic instability). A convenient way to write this term is to formulate it as an advection of the ensemble averaged buoyancy by the eddy induced velocity

$$\mathcal{R} = -\boldsymbol{u}^* \cdot \nabla \overline{b},\tag{16}$$

with

$$\boldsymbol{u}^* = -\nabla \times \frac{\overline{\boldsymbol{u}'\underline{b}'} \times \nabla \overline{\underline{b}}}{|\nabla \overline{\underline{b}}|^2},\tag{17}$$

the non divergent eddy induced velocity, if we only retain the isopycnal component of the eddy flux (Zhao & Vallis, 2008). If we further neglect the horizontal gradient of buoyancy compared to the vertical gradient of buoyancy, we get

$$\boldsymbol{u}^* = (\partial_z \boldsymbol{\Upsilon}, -\nabla_h \cdot \boldsymbol{\Upsilon}), \tag{18}$$

DEREMBLE ET AL. 5 of 25

with $\chi = (\chi^x, \chi^y)$, the eddy-induced transport (see Ferrari et al., 2010)

$$\Upsilon = -\frac{\overline{\underline{u}_h'\underline{b}'}}{N^2}.$$
(19)

Gent and McWilliams (1990) proposed a parameterization of this eddy induced transport in the form of

$$\Upsilon^{\text{GM}} = \kappa \frac{\nabla \bar{b}}{N^2} \tag{20}$$

with κ an eddy induced diffusion coefficient.

One goal of our analysis is to propose an alternative form to the GM parameterization by explicitly computing the eddy induced transport as in Equation 19.

2.4. Eddy Induced Transport in the QG Model

With the MSQG model, one can indeed compute \overline{ub} (with u and b now QG variables) which can then be used to compute the eddy induced transport as

$$\Upsilon = -\frac{\overline{ub}}{N^2}.\tag{21}$$

For a small number of vertical levels in the QG implementation, the eddy induced transport will only capture the low baroclinic modes dynamics which is what modern GM parameterizations are actually aiming at (Ferrari et al., 2010). Note also that the eddy induced transport Υ vanishes at the lower and upper boundaries (because b=0 by construction in the QG model) such that there is no transport across these boundaries (as required). Once we know the eddy induced transport, we can compute the eddy induced velocity that we can then use to compute \mathcal{R} in the coarse resolution model.

An alternative approach is to compute R directly as

$$\mathcal{R} = -\nabla \cdot \overline{u}\overline{b}.\tag{22}$$

such that we skip the step to compute the eddy induced transport. For this approach, we can either directly compute $\nabla \cdot ub$, or we can use the filtering term in Equation 8. Let us elaborate the latter approach: we first note that in a statistically steady state, time averaging Equation 8 results in

$$\overline{\mathcal{F}}_{q} = -\nabla \cdot \overline{uq}. \tag{23}$$

One can convert this PV forcing term $\overline{\mathcal{F}}_q$ into a stream function forcing via Equation 4

$$\overline{\mathcal{F}}_{a} = \nabla^{2} \overline{\mathcal{F}}_{w} + \Gamma \overline{\mathcal{F}}_{w} \simeq \Gamma \overline{\mathcal{F}}_{w}, \tag{24}$$

where $\overline{\mathcal{F}}_{\psi}$ is the large-scale stream function forcing. Hence, if we know $\overline{\mathcal{F}}_{q}$, we can compute $\overline{\mathcal{F}}_{\psi}$ by solving the elliptic Equation 24. Note that since $\overline{\mathcal{F}}_{q}$ and $\overline{\mathcal{F}}_{\psi}$ are large-scale fields, the horizontal Laplace operator in Equation 24 is negligible compared to the vertical stretching term as expected from the scale separation. And last, once we know $\overline{\mathcal{F}}_{\psi}$, we can compute the large-scale buoyancy forcing (see Equation 6).

$$\overline{\mathcal{F}}_b = f \frac{\partial}{\partial z} \overline{\mathcal{F}}_{\psi},\tag{25}$$

This buoyancy forcing corresponds the average effect of eddies on the large-scale buoyancy and is precisely the meaning of the term \mathcal{R} in Equation 1b

$$\overline{\mathcal{F}}_b = \mathcal{R} = -\nabla \cdot \overline{\boldsymbol{u}} b. \tag{26}$$

We will compute R with both methods in the next section and discuss the pros and cons of each strategy.

DEREMBLE ET AL. 6 of 25

2.5. GM Parameterization and PV Homogenization

To close this section on the GM parameterization, we note that in the limit of scale separation between the eddy scale and the gyre scale, buoyancy eddy fluxes and PV eddy fluxes are related via

$$\overline{uq} = f \frac{\partial}{\partial z} \frac{\overline{ub}}{N^2},\tag{27}$$

where the PV flux corresponds in fact to a thickness flux (Treguier et al., 1997) (all variables are QG variables). In the GM parameterization, the buoyancy flux is parameterized as a down gradient flux (see Equations 19 and 20) and can be written in the QG formalism as

$$\overline{ub} = -\kappa \nabla B, \tag{28}$$

with κ the QG eddy diffusivity coefficient. If we combine Equations 27 and 28 and use the definition of the gradient of large-scale PV (Equation 12), we obtain the QG form of the GM parameterization

$$\overline{uq} = -\kappa \overline{\nabla} O, \tag{29}$$

where we have included the β effect in order to write the gradient of the large-scale PV. Equation 29 states that the role of the eddies is to homogenize the large-scale PV because when we take the divergence of the rhs of Equation 29, we get a diffusion operator. This property was originally recognized by Rhines and Young (1982) in an idealized context. In Rhines and Young's experiment, they had a large-scale baroclinic input to the PV but the only component to the large-scale PV gradient was β . They did verify that in a double gyre configuration, PV was well homogenized in regions of high eddy activity (mostly the intergyre) and we can now proceed to a similar verification in a more realistic configuration.

3. Application to a Mid-Latitude Basin

3.1. Reference Case With the Primitive Equation Model

Before we focus on the MSQG model, we first construct a full eddy resolving model that will serve as a reference case against which we will compare the eddy statistics of the simplified model. The configuration of the reference model is directly inspired from Samelson and Vallis (1997b), although we deploy it in an eddy resolving configuration in a similar way to Grooms and Kleiber (2019). With such model, we both capture the large-scale dynamics and the meso-scale eddy dynamics of an extra-tropical basin (idealized version of the North Atlantic Ocean). Equations 1a-1d are integrated forward in time with the MITgcm (J. Marshall et al., 1997) in a square domain (β -plane) of dimension $L \times L$, with L = 5,000 km, and maximum depth H = 4,000 m away from the shelves (see Equation 32). We use a uniform horizontal resolution of 5 km (1,024 points in each horizontal direction), and we use a stretched vertical grid of 52 levels with maximum resolution near the surface (11 m) and minimum resolution near the bottom (274 m). Note that the horizontal resolution of 5 km corresponds to several grid points per deformation radius in most of the domain but we do not expect to resolve well the turbulence in the northern part of the domain where the deformation radius is of the order of 5–10 km. The Coriolis parameter is a function of latitude $f = f_0 + \beta(y - y_m)$ with f_0 the mean value of the Coriolis parameter $f_0 = 8 \times 10^{-5} \sim s^{-1}$, $\beta = 2 \times 10^{-11}$ m⁻¹ s⁻¹, and y_m the mean latitude.

The model is forced at the surface with wind and buoyancy fluxes. The wind stress profile has a zonal component only

$$\mathcal{T}^{x} = -\tau_0 \frac{f}{f_0} \sin\left(\frac{2\pi y}{L}\right),\tag{30}$$

with $\tau_0 = 0.08$ N m⁻². As in Samelson and Vallis (1997b), we choose this wind profile to ensure that there is no Ekman flow at the northern and southern boundaries. The buoyancy fluxes are a relaxation to a prescribed buoyancy profile with uniform meridional temperature gradient of 30 K/5,000 km. The relaxation time scale is set to

$$T_b = \frac{\rho_0 C_p h_0}{O} \tag{31}$$

DEREMBLE ET AL. 7 of 25

with $\rho_0 = 1,000 \text{ kg m}^{-3}$ the constant density of water, $C_p = 4,000 \text{ J kg}^{-1} \text{ K}^{-1}$ the heat capacity of water, h_0 the thickness of the upper grid point of the model and $Q = 35 \text{ W m}^{-2} \text{ K}^{-1}$ a prescribed amplitude of the heat flux such that the relation time scale is on the order of 40 days for the upper 30 m of the ocean.

Along each meridional and zonal boundary, we use a bathtub-like topography (Salmon, 1994) with a shelf given by

$$h_s \exp\left(-\frac{x_n^2}{2d^2}\right),\tag{32}$$

with x_n the coordinate normal to the boundary, d = 200 km the width of the shelf, and $h_s = 2,000$ m the height of the shelf (with respect to the bottom). This topography drastically affects the dynamics of the western boundary current (Jackson et al., 2006; Stewart et al., 2021): it exerts a control on the width of the western boundary current, and on the stability of the separation point.

We plot in Figure 1a the mean stream function Ψ which corresponds to the rotational part of the mean flow and is defined as

$$\nabla^2 \Psi = \frac{\partial \overline{v}}{\partial x} - \frac{\partial \overline{u}}{\partial y} \tag{33}$$

averaged over the upper 172 m and with $\Psi=0$ boundary condition on the sides. With the chosen wind profile, the circulation corresponds to a big anticyclonic gyre (reminiscent of the subtropical gyre) and one smaller cyclonic gyre near the southern boundary. The flow in the western boundary is intensified with a maximum transport of 11 Sv. The strength of this circulation decreases with depth (not shown). The corresponding surface temperature field is plotted in Figure 1b (we recall that temperature is linearly related to buoyancy—see Equation 2). This temperature map exhibits a large-scale north-south gradient, as expected from the atmospheric forcing. A warm core western boundary current is present and hugs the topography up to the northern boundary. We compute the first deformation radius to emphasize the separation of scale between the eddy scale and the gyre scale (Figure 1b). The deformation radius varies between 50 km near the southern boundary to 5 km at the northern boundary.

Vertical sections of temperature shown in Figure 1c are taken in the middle of the domain (y = 2,500 km for the zonal section, and x = 2,500 km for the meridional section). The thermocline which separates the deep ocean from the ventilated layers is visible in the north-south section. The depth at which the internal boundary layer is found is set by the wind forcing (Samelson & Vallis, 1997b). Near y = 3,000 km we see a pool of weakly stratified water that is reminiscent of the subtropical mode water (Deremble & Dewar, 2013). In this model, it is not clear whether this mode water is maintained by a surface buoyancy flux or the Ekman flow convergence at the surface (Dewar et al., 2005). An unstratified deep ocean is a characteristic feature of closed basin models. It is indeed the circumpolar gap that affects the deep stratification (Toggweiler & Samuels, 1995; Warren, 1990).

We plot in Figure 2 a snapshot of specific eddy kinetic energy defined as

$$EKE = \frac{1}{2} (u'^2 + v'^2), \tag{34}$$

and the time mean specific eddy kinetic energy in the upper part of the ocean. As expected, we observe an intense eddy activity that is maximum near the western boundary. This maximum of EKE follows well the isobath contours and so executes a sharp turn in the north west corner (as does the mean flow). There is a relative maximum of EKE near the 4,000 km latitude which corresponds approximately to the zero wind stress curl line. Near the northern boundary, there is evidence of a permanent zonal jet strongly anchored above the topographic shelf (a well known feature for β -plane turbulence; see e.g., Simonnet et al., 2021). There is little eddy activity in the southern part of domain. As we shall see in the next section, most of this eddy activity can be explained by the baroclinic instability of the mean flow. Last, in order to examine how the eddies rectify the mean flow, we plot both components of the eddy induced transport Υ in Figure 3. Both Figures 2 and 3 will serve as a reference to which we will compare the QG model. Note that we plot the smoothed version where we average 8×8 neighboring grid points and linearly interpolate back on the fine grid for visualization purposes. All smoothed fields are smoothed this way.

DEREMBLE ET AL. 8 of 25

19422466, 2023, 10, Downloaded from https://agupubs.onlinelibrary.wiley.com/doi/10.1029/2022MS003572 by Florida State University, Wiley Online Library on [06/06/2024]. See the Terms and Conditions

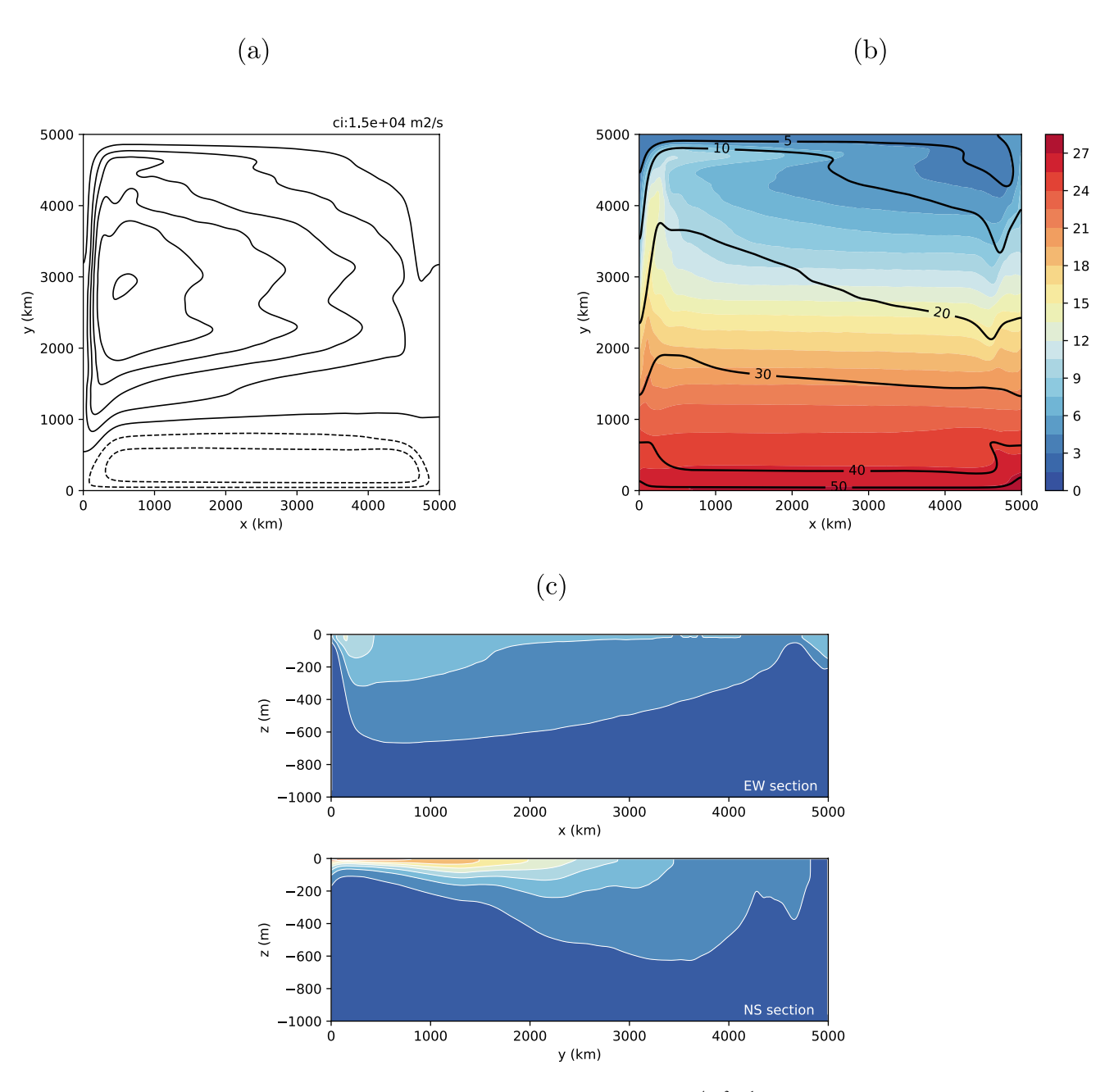


Figure 1. (a) Time mean stream function Ψ averaged over the upper 172 m. Contour interval is 1.5×10^4 m 2 s $^{-1}$. (b) Time mean Sea surface temperature (colors) and first deformation radius (contours, unit: km). (c) Time mean Vertical temperature profiles in the middle of the domain for the upper 1,000 m. Top: north-south section. Bottom: east-west section. The colorbar is the same for panels (b) and (c) (unit $^{\circ}$ C).

This configuration corresponds to the reference case where both the mean flow and the eddies are well captured by the model. The question we are asking is whether we can take the mean flow of this configuration, pretend it comes from a coarse resolution model, and set up a model of intermediate complexity that is cheaper to run than the full eddy resolving model, but that can still capture the eddy variability and eddy fluxes on the mean flow. To illustrate this approach, we use the MSQG model that we described in Section 2.2.

3.2. Results of the MSQG Model

We integrate the MSQG model (Equation 8) forward in time starting from rest in the same physical domain as the reference model. We use four vertical levels of thickness h = 172, 359, 936,and 2,531 m from top

DEREMBLE ET AL. 9 of 25

19422466, 2023, 10, Downloaded from https://agupubs.onlinelibrary.wiley.com/doi/10.1029/2022MS003572 by Florida State University, Wiley Online Library on [06/06/2024]. See

litions) on Wiley Online Library for rules of use; OA articles are governed by the applicable Creati

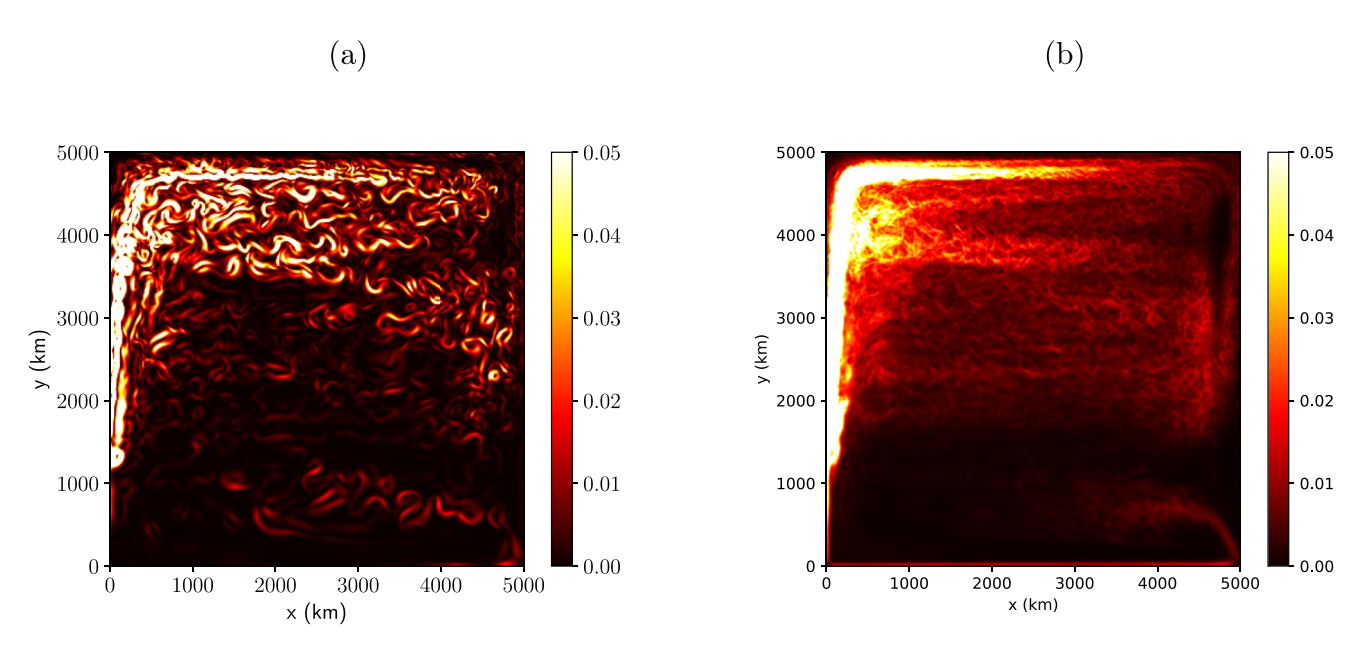


Figure 2. (a) Snapshot of specific eddy kinetic energy (unit: m² s⁻²). (b) Mean specific eddy kinetic energy (unit: m² s⁻²). Both fields are averaged over the upper 172 m of the primitive equation model.

to bottom. We recall that $f_0 = 8 \times 10^{-5}$ and $\beta = 2 \times 10^{-11}$ m⁻¹ s⁻¹ which corresponds to a Rossby number $Ro = u_s/fl_s$ between 0.015 and 0.067 in the northern and southern part of the domain respectively (with $u_s = 0.1$ m s⁻¹, and $l_s = 50$ km, the characteristic velocity and length scale). We use a bi-harmonic viscosity coefficient $A_4 = 10^{10}$ m⁴ s⁻¹ which correspond to a bi-harmonic Reynolds coefficient $Re_4 = 1,250$ (with $Re_4 = u_s l_s^3/A_4$). We set a bottom drag coefficient with a spin down time scale of $r^{-1} = 146$ days. This corresponds to an Ekman layer of thickness $\delta_E = 2rh_l/f_0 = 5$ m (with h_l the thickness of the bottom layer) or a value of the Ekman number $\delta_E/H = \sqrt{v_v/f_0H^2} = 1.25 \times 10^{-3}$, which also corresponds to a turbulent vertical viscosity in the bottom boundary layer of $\nu_v = 3 \times 10^{-3}$ m² s⁻¹. The filter \mathcal{F}_q works exactly as in Uchida et al. (2022): every 2 days, we proceed to a wavelet decomposition of the stream function and we subtract the component of this field that is larger than 550 km (roughly five times the instability length scale). The

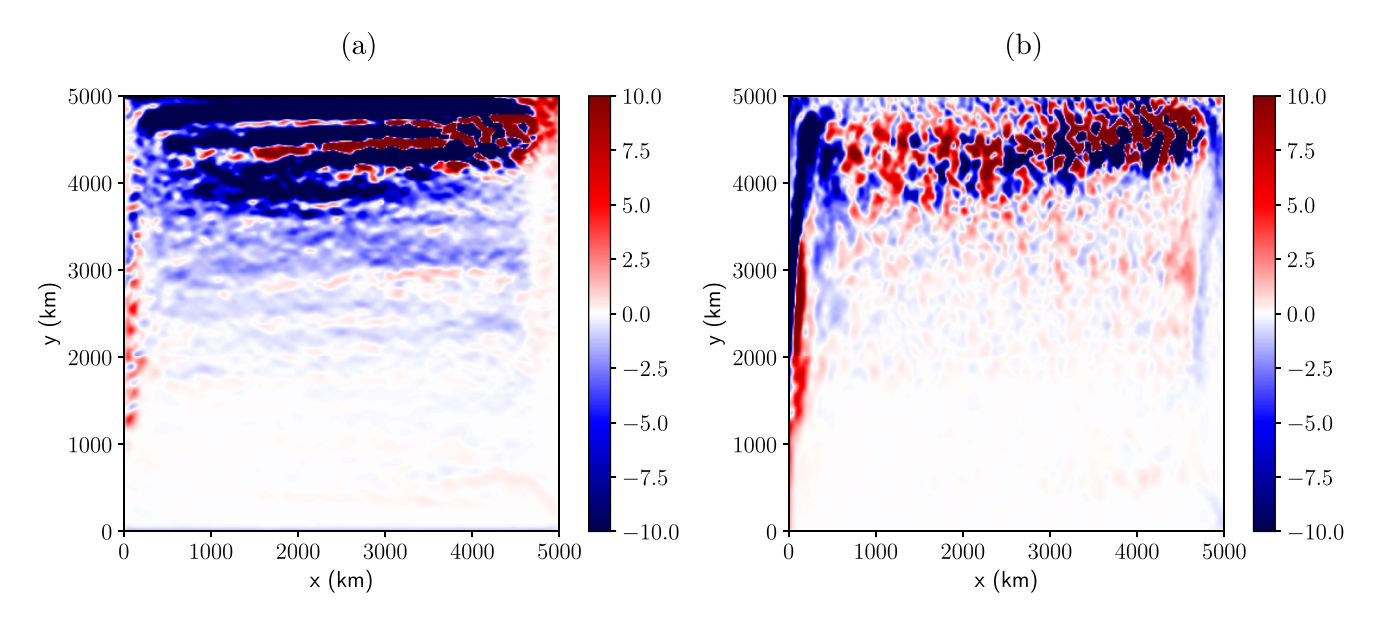


Figure 3. (a) Zonal component, and (b) meridional component of the eddy induced transport Υ , as defined in Equation 19 for the primitive equation model averaged in the upper 172 m. Both fields are smoothed by averaging nearby points (see text) (unit: m² s⁻¹).

DEREMBLE ET AL. 10 of 25

total length of the time series is 40 years and the outputs are 30-day snapshots. The imposed large-scale stream function Ψ is computed by solving at each level the 2D Poisson equation (Equation 33) where the time averaged relative vorticity of the PE model is vertically coarse grained on the four QG levels (illustration of the upper level stream function is given in Figure 1). With such large-scale stream function, we can compute the large-scale velocity U and V as shown in Equation 10. In a similar way, to compute the Brunt-Vaisala frequency N^2 , we first compute the time mean buoyancy field B of the PE model. We then coarsen this field in the vertical dimension on the four QG levels. Last, we take the vertical derivative of the latter field to get N^2 at the interface between QG levels (in the usual vertical discretization of QG models, see Cushman-Roisin & Beckers, 2011).

In the first days of the time integration, we first observe a transient phase during which the most unstable modes grow. These most unstable modes have a local wavelength that varies in space simply because the hydrographic properties of the large-scale flow and the Coriolis parameter vary in space. Obviously the time scale of the instability is also a function of space such that all parts of the domain do not stay in the transient phase for the same amount of time. As time increases the amplitude of the linear waves saturate and the system evolves into a fully non-linear state. Because we filter the large-scale part of the dynamics, we force the system to stay in an unstable regime that we call a statistically stationary eddying state. With this strategy, we can achieve long integrations of the eddy field for a given background flow and we can analyze meaningful statistics of eddy fluxes for such mean flow. Henceforth, we only analyze the last 33 years which are in statistical steady state.

3.3. Energetics of the Small-Scale Flow

Oceanic eddies carry both kinetic energy defined in the QG formalism as

$$E_k = \frac{1}{2} \left(u^2 + v^2 \right) = \frac{1}{2} (\nabla \psi)^2 \tag{35}$$

and potential energy defined as

$$E_p = \frac{1}{2} \frac{b^2}{N^2} = \frac{1}{2} \frac{f^2}{N^2} \left(\frac{\partial \psi}{\partial z} \right)^2$$
 (36)

We plot in Figure 4 snapshot of kinetic energy E_k and mean kinetic energy $\overline{E_k}$. As already observed for the reference case, there is a vigorous eddy field, well pronounced in the western and northern part of the subtropical gyre. The zones of maximum eddy activity do not necessarily correspond to the zones of maximum growth rate for the barotropic/baroclinic instability (not shown). We recall that the origin of this eddy field is only the baroclinic instability but that eddies can travel in and out of unstable regions. We recover that there is much more kinetic energy in the eddy flow than in the background flow: in the snapshot of E_k (Figure 4a), one can see the rings, jets, and filaments with maximum velocity on the order of 1 m s⁻¹ for the most energetic structures (whereas the background kinetic energy is much weaker and localized in the western boundary, not shown). Patterns of potential energy tend to fill the holes of the KE patterns (not shown). The plot in Figure 4 compares well with the reference case both for the snapshot and the mean field. We emphasize again that we only have 4 levels in the QG model (compared to the 52 levels in the PE model) and only one dynamical variable (compared to 3 in the PE model). We have also computed the time evolution of the PV field with a traditional QG model (uniform N^2 and uniform f in the definition of PV—but still with the traditional f effect) and got a poor agreement with the reference case (see Appendix A).

The total kinetic energy in the QG model is 0.2 EJ (1 EJ = 10^{18} J), whereas the total potential energy is 0.7 EJ—we have multiplied the kinetic and potential energy in Equations 35 and 36 by a constant $\rho_0 = 1,000$ kg m⁻³ and integrated over the whole domain to get energies in Joules. So we get the same order of magnitude for the kinetic and potential energy which is consistent with the QG scaling and the fact that we operate at Burger number close to one. To put these numbers in perspective, we can compare these energies with the energy in the large-scale solution: there is 22 EJ of available potential energy (APE) and 0.08 EJ of mean kinetic energy which is all consistent with the energy partition in the ocean (Vallis, 2017). As expected, we have the eddy kinetic energy and eddy potential energy orders of magnitude smaller than the mean APE: there is only a small fraction of the large-scale energy reservoir that is drained in the eddy field. We also note that the amount of energy contained in

DEREMBLE ET AL. 11 of 25

19422466, 2023, 10, Downloaded from https://agupubs.onlinelibrary.wiley.com/doi/10.1029/2022MS003572 by Florida State University, Wiley Online Library on [0606/2024]. See

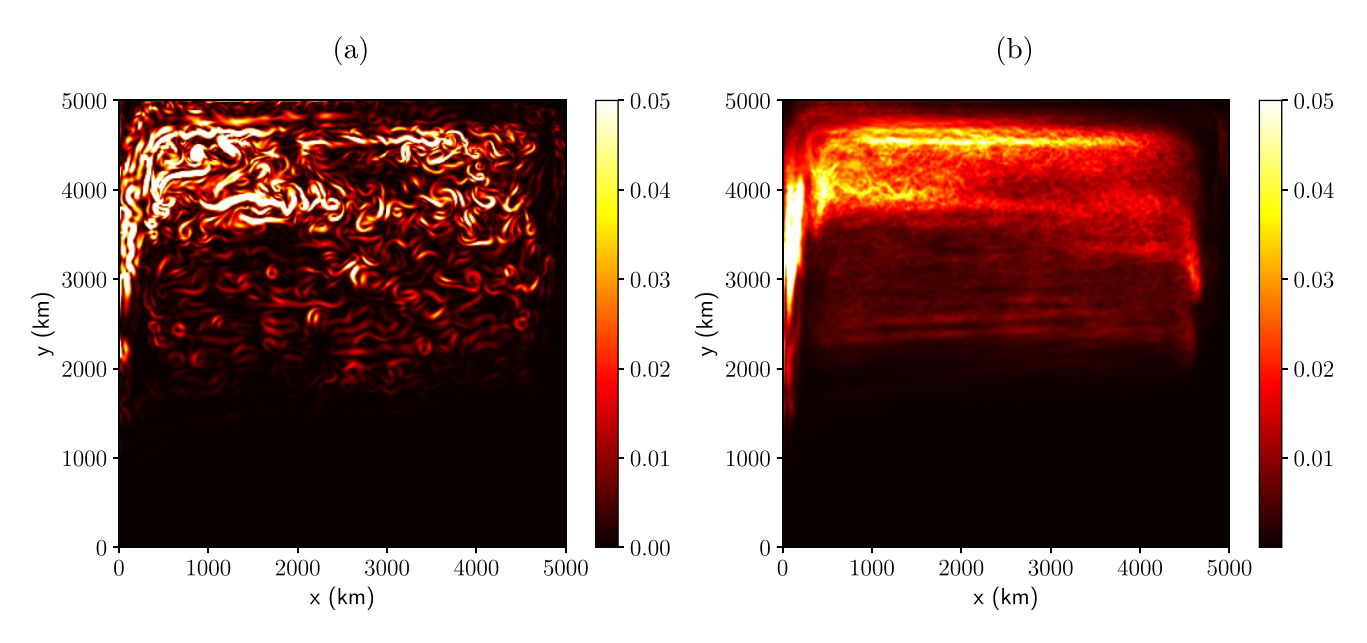


Figure 4. (a) Snapshot of the Quasi-Geostrophic (QG) kinetic energy E_k in the upper level; (b) mean kinetic energy $\overline{E_k}$ in the upper level (Same as Figure 2 but for the QG model).

the mesoscale field is consistent with the number of 13 EJ discussed by Wunsch and Ferrari (2004) for the global eddy energy, given that we study only one gyre and that most of the global EKE is in the ACC.

To get the energy equation of the small-scale flow, we multiply the equation of evolution of PV (Equation 8) by $-\psi$ and integrate over the entire domain

$$\frac{\partial E_k + E_p}{\partial t} = \underbrace{\int_{\Omega} (-vUq + uVq) d^3x}_{\text{BI}} - \underbrace{\int_{\Omega} \psi \mathcal{D}_q d^3x}_{\text{SD+BF}} + \underbrace{\int_{\Omega} \psi \mathcal{F}_q d^3x}_{\text{IC}} + \text{res.}$$
(37)

The three terms in the rhs of Equation 37 are respectively the energy input via baroclinic and barotropic instability (BI), the sum of the small-scale dissipation and bottom friction (SD + BF), and the effect of the filter that damps large-scale structures that are created via IC and are the leading order terms in the MSQG model. In the multiple scale formalism, the other terms of the energy equation (advection of small-scale energy by the small-scale flow and advection of large-scale energy by the small-scale flow) do not exactly vanish in the numerical model and are gathered here in the residual term in Equation 37 (see discussion at the end of this section and Appendix B). In a statistical steady state, the leading order balance is between the three terms in the rhs of Equation 37: this corresponds to the classical paradigm where eddies are generated via baroclinic and BI and energy is dissipated

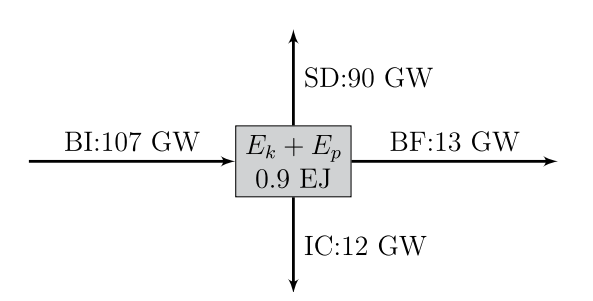


Figure 5. Energy budget of the multiple-scale Quasi-Geostrophic model. The unit of the energy reservoir is in EJ (1 EJ = 10^{18} J) and the unit of the energy flux is GW (1 GW = 10^9 W). BI, baroclinic instability; IC, inverse cascade; BF, bottom friction; SD, small-scale dissipation.

by viscous and diffusive processes plus a moderate IC that is halted by BF. In such a scenario, eddies do not feedback on the large-scale flow (IC = 0). We show here that, indeed, the eddy feedback on the large-scale flow is weak. It is on the same order of magnitude as BF, but this term is key to maintain the eddy structure close to the reference run: we also ran the MSQG model without the filtering term and we obtained a different eddy field superimposed to a spurious large-scale flow (see Appendix A and Uchida et al., 2022).

We summarize in Figure 5 the energy budget of the QG model in the configuration that we discussed in the previous section. The QG flow finds its energy in the large-scale APE that drives the baroclinic instability. This corresponds to an energy flux of BI = 107 GW. This energy is dissipated via three mechanism: viscous and diffusive dissipation removes energy at the smallest scales (SD = 90 GW), BF dissipates 13 GW and the filter dissipates large-scale structures at a rate of 12 GW. For the SD term, we recall that it is written

DEREMBLE ET AL. 12 of 25

as a bi-harmonic operator acting on both the relative vorticity component and the vortex stretching component. Hence, SD corresponds to the sum of a kinetic energy sink and a potential energy sink. The decomposition of this term in these two components reveals that 78 GW correspond to a potential energy loss whereas 12 GW correspond to a kinetic energy loss. Last, we state again that even if BF and IC are weak, they are key processes to maintain a realistic eddy flow. We also note that in a preliminary work where we used a real PG solution for the large-scale flow (as originally derived in Pedlosky, 1984), the IC term was actually the leading order term in the energy balance. This is because the PG flow was strongly baroclinically unstable. In the PG formalism, we tame these instabilities with friction and viscosity (Colin de Verdiere, 1986; Samelson & Vallis, 1997a) but if we use this flow as a background state for the QG model, then eddies quickly erode the stratification such that the leading order term corresponds to this erosion.

Finally, we state that the energy budget is not perfectly closed (approximately 7% residual). This is an intrinsic property of the multiple scale QG model where N^2 varies in space and such that the model does not conserve potential energy. Consider for instance a vortex that carries both kinetic and potential energy. If the vortex is advected in another location, in the QG formalism, it will conserve its kinetic energy but its potential energy will vary simply because N^2 varies in space (see Equation 36). The only way to minimize this drawback is to use a smooth background buoyancy frequency. In the limit where N^2 is constant, then the model conserves both kinetic and potential energy (see derivation in Appendix B). From a numerical perspective, we were able to close the energy budget (less than 1% residual) when keeping track of all the terms that vanish in the traditional QG formalism but do not vanish in the multiple scale formalism (namely $yu \cdot \nabla q$ and $wu \cdot \nabla Q$).

Given that the global energy input by wind to the large-scale circulation is O(1 TW) (Jamet et al., 2021), our estimate of dissipation in a single gyre of 100 GW does not seem irrelevant. However, any comparison with the real ocean should be taken with a grain of salt for three reasons: first, QG dynamics are missing many important phenomena (mixed layer dynamics, unbalanced dynamics) that could affect the energy balance. Second, the topography is clearly not realistic and the flow-topography interaction is not well represented in QG (Deremble et al., 2017). And last, the variability of the forcing could trigger a seasonal response in the eddy statistics that is not represented here (see Uchida et al., 2021).

4. Rectification Term

We now focus on the eddy correlation terms in order to advance toward a parameterization of mesoscale eddies. As a starting point, we analyze the impact of eddies on the mean PV. Then we compute the eddy induced transport and compare this quantity to what was obtained in the reference case. Last, we discuss the variability of the rectification.

4.1. Effect on Potential Vorticity

To demonstrate the impact of the eddies on the large-scale PV, we plot in Figure 6 $\nabla \cdot \overline{ua}$ and the average rectification term \overline{F}_a taken over a 33 years long time series. We chose the color scale in order to see the patterns of these fields in most of the domain (the colorbar saturates in the northern part of the domain where f is big and N^2 is small). These two plots should be identical according to Equation 23, but in fact, the time series of the model is not long enough for the mean to converge. Also, we recall that \mathcal{F}_a is really a parameterization for $\nabla \cdot \overline{ua}$ that we approximate with a spatial filter (see Equation 14) and this parameterization is not perfect as shown in Uchida et al. (2022). Nevertheless, the maxima in these two plots are located at similar geographical locations and the two plots seem to differ from one another by small-scale structures and also near the boundaries. As we approach the boundary we enter a region for which the length scale of the most unstable mode is bigger than the distance to the boundary (not shown). It is clearly a region where we do not expect the filtering strategy to work well. In most of the domain, the balance (Equation 23) is helpful because it means we can use either $\nabla \cdot \overline{uq}$ or \overline{F}_q to build a parameterization of mesoscale eddies. In order to estimate the eddy diffusivity κ (see Equation 29), we compute the scalar product $\nabla Q \cdot \overline{uq}/|\nabla Q|^2$ that we plot in Figure 7. One key result is that the eddy flux of PV is mostly downgradient as illustrated by the fact that this figure is mostly red. Note also that the mean eddy PV flux is dominated by the stretching component. In regions where κ is positive, we estimate the magnitude of the eddy diffusivity coefficient to be $\kappa \sim O(10^3 - 10^4) \text{ m}^2 \text{ s}^{-1}$. This is not meant to be an exact number but rather an order of magnitude of the eddy diffusivity. This value is well in the range of values used for eddy diffusivity diagnosed

DEREMBLE ET AL. 13 of 25

19422466, 2023, 10, Downloaded from https://agupubs.onlinelibrary.wiley.com/doi/10.1029/2022MS003572 by Florida State University, Wiley Online Library on [06/06/2024]. See

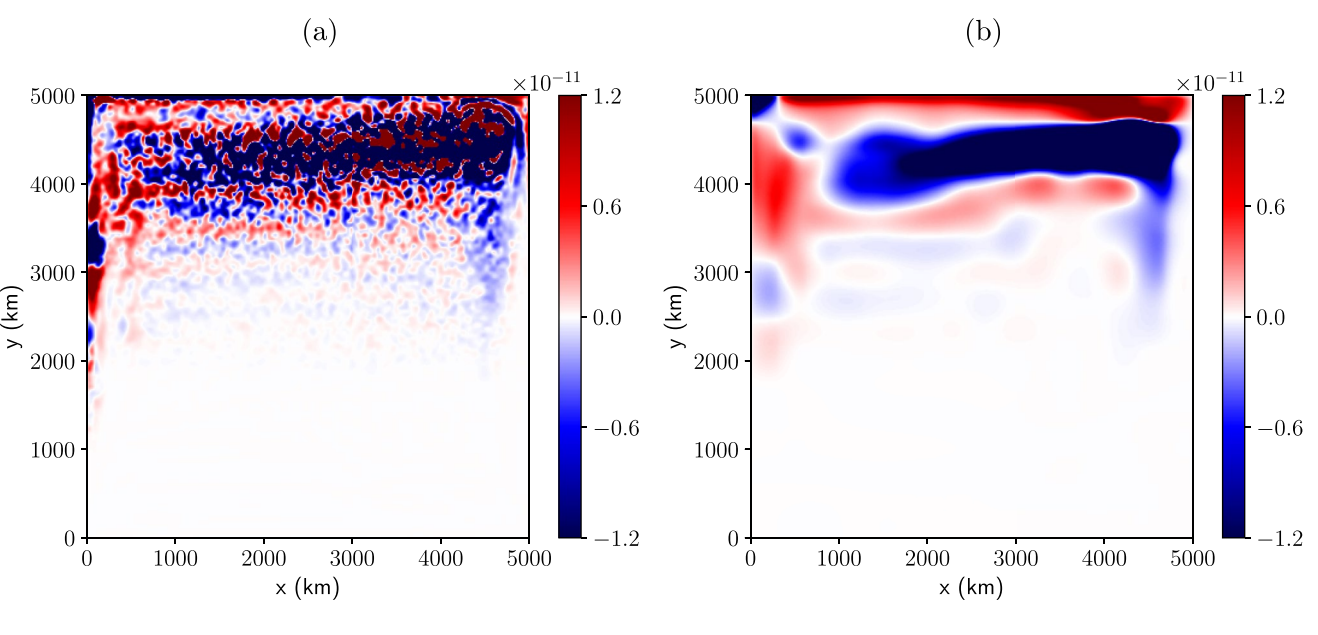


Figure 6. (a) $-\nabla \cdot \overline{uq}$ (smoothed), (b) $\overline{\mathcal{F}}_q$ for the multiple-scale Quasi-Geostrophic model forced with the mean flow of the primitive equation model (units are s⁻²).

in high resolution models (Abernathey et al., 2013; Uchida et al., 2023) and used in low resolution ocean models (Nakamura & Chao, 2000). There are zones with upgradient PV flux near the western boundary (a region of intense eddy activity) and in banded structures in the middle of the domain. The impact of this up-gradient PV flux is to sharpen the large-scale PV gradients.

The horizontal and vertical structure of κ is not uniform (see also Abernathey et al., 2013). Overall the magnitude of κ decreases with depth. In the second and third levels, there are large areas where κ is weakly negative (not shown).

4.2. Impact of the Eddies on the Mean Buoyancy Field

Ultimately, we want to parameterize the effect of eddies on the mean buoyancy (term \mathcal{R} in Equation 1b). As mentioned earlier, there are three strategies to build this parameterization: (a) we can compute the eddy induced

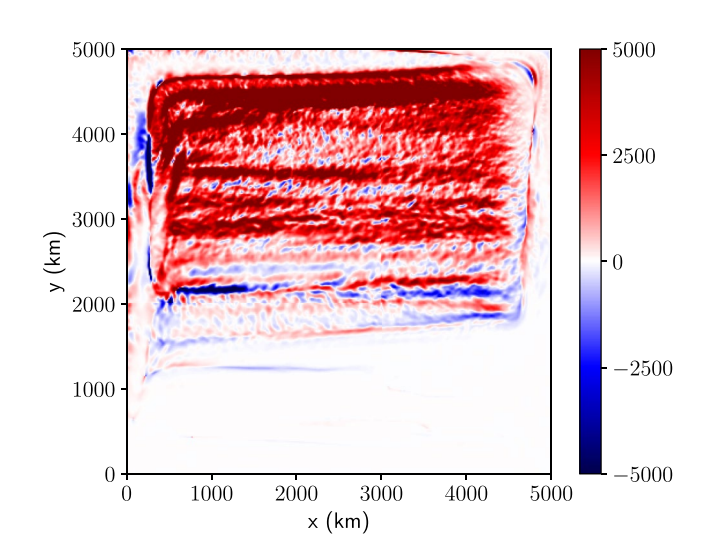


Figure 7. Eddy diffusivity coefficient κ diagnosed as $\overline{\nabla}Q \cdot \overline{uq}/|\overline{\nabla}Q|^2$ in the upper level (units are m² s⁻¹).

transport in the QG model and use the eddy induced velocity field in the PE coarse resolution model to advect the temperature and salinity fields (and also other tracers), (b) we can compute $\nabla \cdot \overline{ub}$ as an estimate of \mathcal{R} , or (iii) we can compute the mean buoyancy forcing $\overline{\mathcal{F}}_b$ as an estimate of \mathcal{R} (see Equation 25).

For the first strategy, we need to compute the eddy induced transport. In the QG framework, this transport is defined in Equation 21. We plot both components of the eddy induced transport Υ in Figure 8. These plots compare well with the reference case (Figure 3): the location and the magnitude of the maxima matches what we had in the full model.

For the second and third strategies, we plot $-\nabla \cdot \overline{ub}$ and $\overline{\mathcal{F}}_b$ in Figure 9. These two terms correspond to the buoyancy forcing term \mathcal{R} and they are not equal simply because we did not run the model for a sufficiently long time, and because the divergence of the eddy buoyancy flux is slower to converge than \mathcal{F}_b (see Figure 10). The plots in Figure 9 illustrate the warming and cooling tendency (if we interpret buoyancy as temperature) due to the eddies on the large-scale solution. We observe alternating cooling and warming patterns in the western boundary and in the gyre which are unfortunately relatively hard to interpret as is. In order to get more physical insight into how this terms acts

DEREMBLE ET AL. 14 of 25

19422466, 2023, 10, Downloaded from https://agupubs.onlinelibrary.wiley.com/doi/10.1029/2022MS003572 by Florida State University, Wiley Online Library on [0606/2024]. See the 7

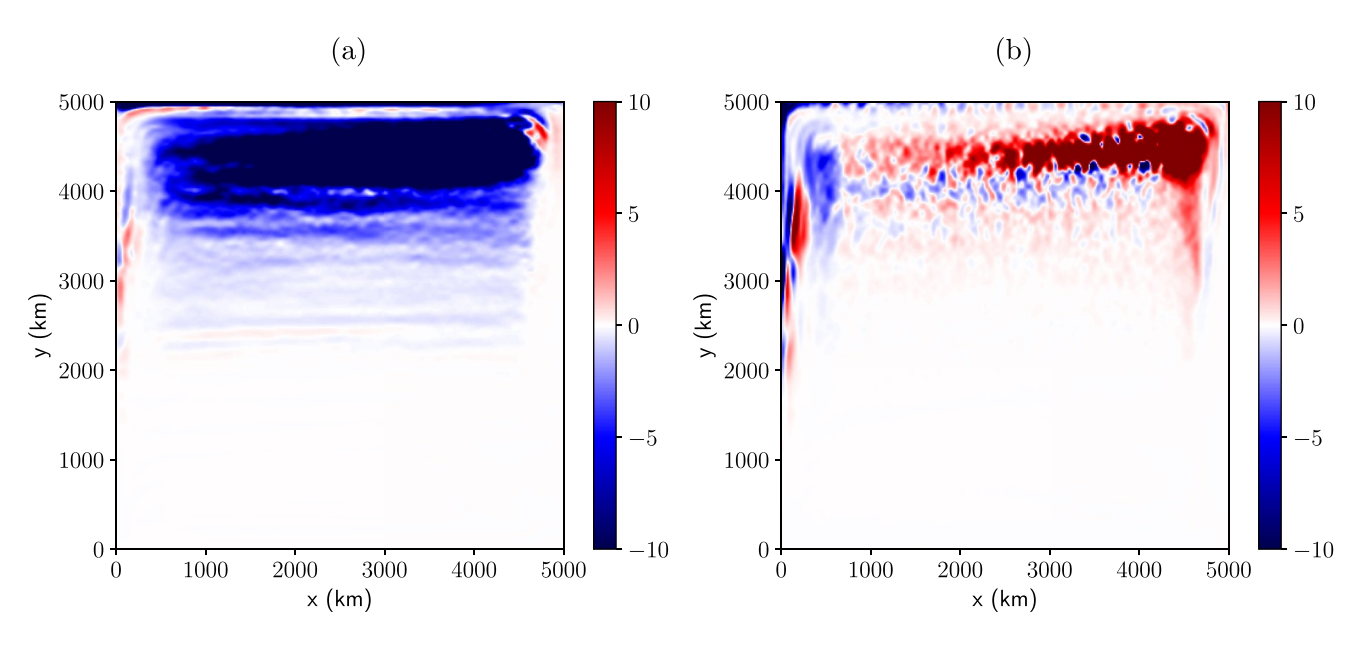


Figure 8. (a) Zonal component and (b) meridional component of the upper layer eddy induced transport Υ in the Quasi-Geostrophic (QG) model, as defined in Equation 21. Units: $m^2 \, s^{-1}$ (Same as Figure 3 but in the QG model).

on the mean flow, we can convert the buoyancy forcing to a temperature forcing: as an indication, the dark blue patch in the western boundary corresponds to a forcing of 4 K/year and the light red patch in the northern part of the gyre corresponds to a temperature forcing of 0.4 K/year.

4.3. Intermittency of the Rectification

With the MSQG model, we are able to diagnose the average rectification term as an alternative to the standard GM parameterizations. But there is actually more information available in the QG dynamics than just the average feedback $\nabla \cdot \overline{ub}$ because the term $\nabla \cdot (ub)$ is a function of time. So far, we have only focused on the time mean rectification. In order to build a rectification term that takes into account this variability, one could use a long time

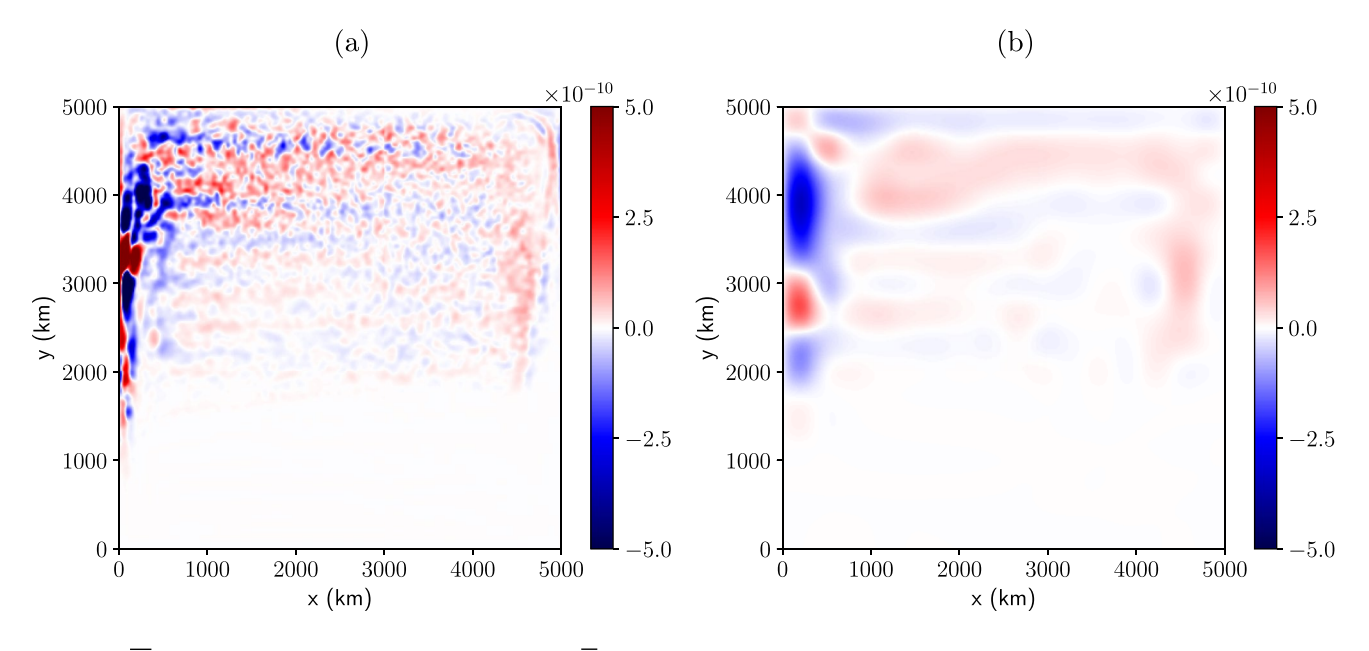


Figure 9. (a) $-\nabla \cdot \overline{ub}$ smoothed in the upper buoyancy level. (b) Color: \overline{F}_b in the same level (units in both plots: m s⁻³).

DEREMBLE ET AL. 15 of 25

19422466, 2023, 10, Downloaded from https://agupubs.onlinelibrary.wiley.com/doi/10.1029/2022MS003572 by Florida State University, Wiley Online Library on [06/06/2024]. See

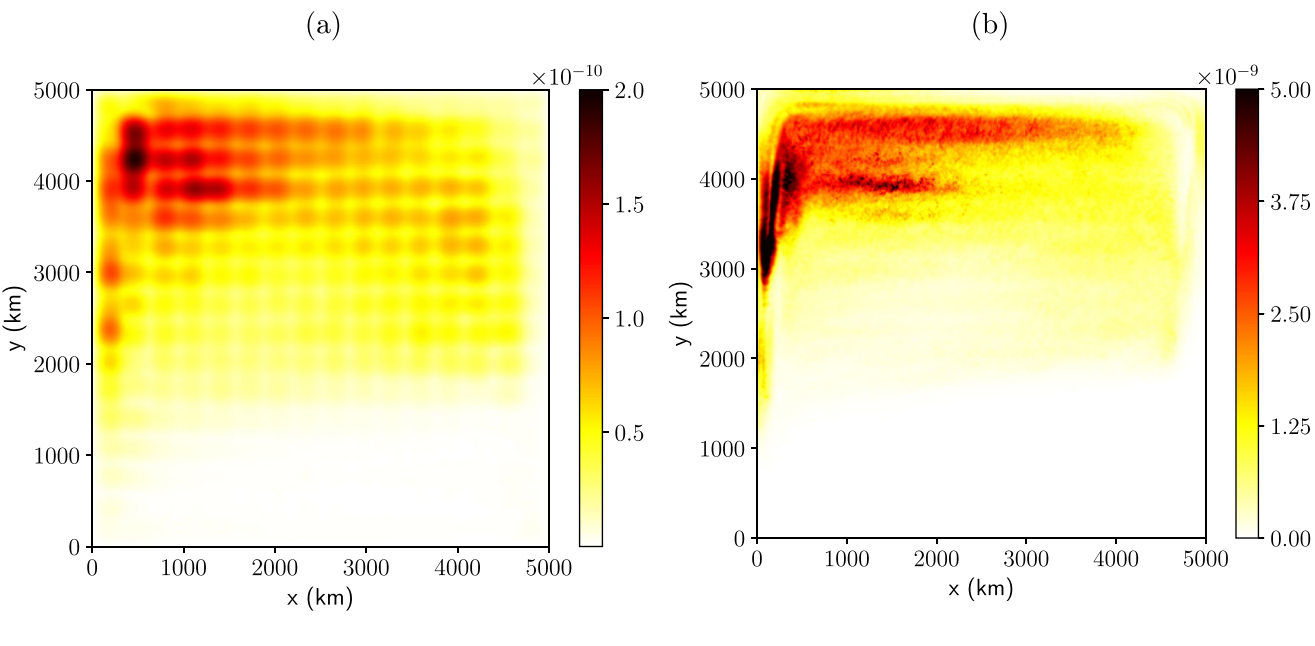


Figure 10. (a) Standard deviation of \mathcal{F}_b and (b) standard deviation of $\nabla \cdot (ub)$ (units m s⁻³).

series of $\nabla \cdot (ub)$ to extract the variability patterns and add one or several modes of this variability to the mean in the rectification term (Li et al., 2023). As a starting point, we document here the first moments of the distribution of the eddy statistics, in a similar way as what was proposed by Grooms (2016) and Grooms and Kleiber (2019).

We first note the auto-correlation of $\nabla \cdot (ub)$ between two consecutive outputs (30 days) is below 0.2 in most of the domain (not shown). Hence, two consecutive output of $\nabla \cdot (ub)$ can be considered close to independent from each other. This result is consistent with Porta Mana and Zanna (2014) who found that the decorrelation time of the eddy rectification term is on the order of days (see also Samelson et al., 2019, for a similar analysis with sea surface height fields). As for any random time series, the time scale needed to build a significant mean depends on the statistical moments of the distribution.

We first plot in Figure 10 the standard deviation of $\nabla \cdot (ub)$ and \mathcal{F}_b . This figure highlights the chaotic regions of the dynamics. These regions are directly related to the high eddy activity in some parts of the domain (see Figure 4). Predicting the location of these zone with a linear instability analysis only (i.e., without the non-linear QG model) seems hard to do: the zones of high eddy variability do not directly correspond to zones of maximum instability growth rate (not shown). In fact regions of high variability extend well beyond the zone with high linear growth rate. This is because once formed, eddies are advected away from their formation site and may drive an IC in sites that are weakly unstable. The discrepancies between the location of the most unstable modes and the location of maximum eddy activity illustrates the fact that the large-scale rectification by the small scale eddies is not necessarily a local process and our strategy of explicitly modeling the small scale variability can capture this effect. These structures also reflect the fact that the IC is not uniform either in space or in time.

The standard deviation of the sample mean is given by σ/\sqrt{n} with n the sample size. We can use this definition to get the error bar on the mean fields that we showed in the previous section. If we focus on \mathcal{F}_b , we see in Figure 9 that the order of magnitude of the mean is $\sim 10^{-10}$ m s⁻³ and in Figure 10 we see that the order of magnitude of the standard deviation of that same field is also $\sim 10^{-10}$ m s⁻³. Since our sample size is 400 points (33 years time series with 30 days output), we estimate that we have 5% error on the field $\overline{\mathcal{F}}_b$. Because the standard deviation of $\nabla \cdot (ub)$ is 20 times bigger than the standard deviation of \mathcal{F}_b and if we consider that the mean should be identical, then the error on the field $\nabla \cdot \overline{ub}$ is on the order of 25%. If we wanted a 5% error on this field, we would need a 1,000 years time series. This time scale is bigger than the thermocline time scale. This implies that eddies could in principle drive low-frequency variability at the thermocline scale and this variability would itself be modulated by the slow evolution of the thermocline (Berloff et al., 2007).

DEREMBLE ET AL. 16 of 25

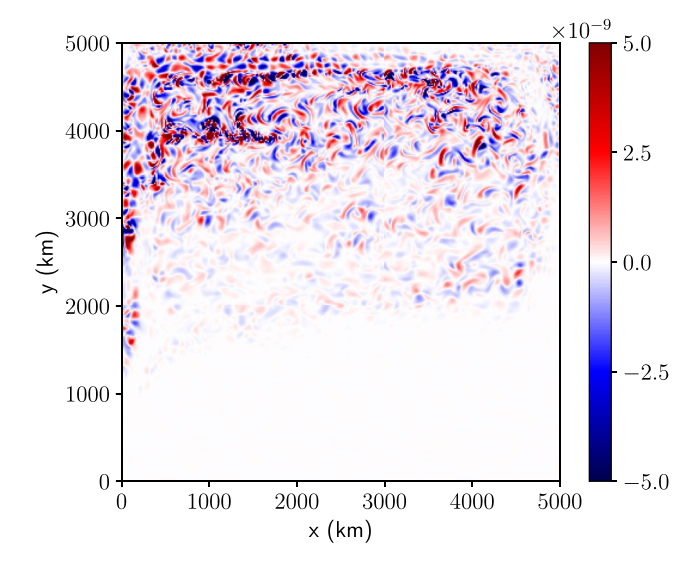


Figure 11. Snapshot of $\nabla \cdot (ub)$ in the upper buoyancy level of the Quasi-Geostrophic model.

There are two ways we can use this information to incorporate elements of the eddy variability in the GM parameterization. Depending on how we want to represent eddies in the coarse resolution model, we can construct a rectification term \mathcal{R} that is anywhere between a snapshot \mathcal{F}_b and the absolute mean $\overline{\mathcal{F}}_b$ depending on the degree of variability that one wish to add to \mathcal{R} and compute the corresponding time varying eddy induced velocity.

If we do not want to implement a QG model, another possibility to get a time variable GM is simply to add noise in the eddy induced transport Υ . With this formulation, we depart from Grooms and Kleiber (2019) because we propose to model the stochastic component of the parameterization as an additive noise. To illustrate the type of noise, we plot in Figure 11 a snapshot of $\nabla \cdot (ub)$. We computed a power spectra of this field a got a curve that is relatively flat in the 50-500 km range and falls off outside of that range (not shown). One possibility to add a stochastic component to GM would be to add to the GM mean a white noise field in this wavelength band. We can further characterize the type of noise with the skewness (S) and excess kurtosis (K) of \mathcal{F}_b . In most of the domain, |S| < 2 and |K| < 2 such that both the skewness and kurtosis are not significantly different from zero. Hence the variability of the rectification could be modeled as a random process normally distributed, we suggest that we can formulate the rectification as a Wiener process where the amplitude of the noise needs to be learned with a series of realizations of the QG model.

5. Conclusion

We implemented a prototype MSQG model for which the large-scale component is described by the average flow of a full eddy resolving model and the small-scale component is described by QG dynamics (Grooms et al., 2011; Pedlosky, 1984). In this context, QG dynamics is solely forced by the baroclinic instability of the large-scale flow. The main originality of this implementation is to deploy the QG model at the basin scale such that the stratification (or equivalently the deformation radii) and the large-scale flow are slowly varying in space. This contrasts with the traditional QG implementation where these large-scale variables (stratification and background flow) are uniform over the QG domain. This new model is well suited to study the full instability problem in ocean gyres: the main advantage of this new implementation is to relax the locality hypothesis which assumes that oceanic eddies are generated locally and interact only locally with the large-scale flow (Tulloch et al., 2011; Venaille et al., 2011). A comparison between the MSQG model and the reference PE model shows good agreement between the two eddy dynamics. We then focused on the different methods to use the QG model to rectify the background flow. In this article, we showed that, the IC remains weak (on the same order as BF). However, the nature of the solution would be different without the large-scale filtering (the same remark applies for BF). The consequence of this IC is that the small-scale flow rectifies the large-scale flow. This claim was also what was anticipated by Gent and McWilliams (1990) when they proposed a parameterization of ocean eddies. In our paper, we have compared GM fluxes with the fluxes computed with a model of intermediate complexity that explicitly resolves eddy dynamics. We find good agreement between the QG model and the reference PE model such that eddies flatten isopycnal surfaces (or homogenize PV) with a diffusivity coefficient on the order of $10^3 - 10^4$ m² s⁻¹. We also showed that in specific places eddies can strengthen the large-scale flow by fluxing PV up the mean gradient. The fact that we could not get a converged field of $\nabla \cdot \overline{ub}$ after 30 years of integration even after applying a spatial smoothing, raises an interesting concern: it is probably pointless to parameterize the eddy as a stationary response. The eddy response inevitably contains a time-variable part that we can capture with the QG model.

This multiple scale model offers many possibilities for process oriented studies. The immediate extension of this work is to study the full super-parameterization implementation where the mean flow comes from a coarse resolution model and the eddy feedback is effectively added to the mean flow. We anticipate that the rectification of the large-scale flow by small scale eddies will have two effects: first it will change the background flow seen by the QG model. This change will modify the strength of the baroclinic instabilities (Farrell &

DEREMBLE ET AL. 17 of 25



Journal of Advances in Modeling Earth Systems

10.1029/2022MS003572

Ioannou, 1999; Flierl & Pedlosky, 2007). But most importantly, it will drive an additional air-sea flux in an attempt to restore the initial large-scale solution. Because we observed strong variability in the rectification process, we conjecture that a coupled model will exhibit low-frequency modes of variability via this mechanism. The coupled model is also well suited to revisit the dynamics of the ventilated thermocline in the presence of eddies and see how the conservation of large-scale PV is modulated by the PV homogenization due to small-scale eddies (Deremble & Dewar, 2013). Eddy-mean flow is also a key interaction in the ACC because a large fraction of the mass and heat transport is carried out by eddies (Cessi et al., 2006). Many conceptual models of the ACC rely on a parameterization of oceanic eddies to establish the vertical structure of the isopycnal layers (J. Marshall & Radko, 2003; Nikurashin & Vallis, 2012). This multiple scale model offers an alternative to these parameterized models and could help validate or adjust theoretical models on the residual circulation in the ACC.

Another aspect that we have only briefly mentioned is the effect of the seasonal cycle. The seasonal time scale is between the eddy time scale and the planetary time scale and should have a strong impact on both systems. In particular, the seasonal cycle will have an impact on the deep convection areas, and will also affect the depth of the mixed layer. These changes may locally enhance the eddy dynamics and thus affect the coupled system. There are possibilities to explore this variability (Uchida et al., 2021). The extension to the MSQG model is clearly possible but is beyond the scope of this study.

Appendix A: Other QG Configurations

A1. MSQG Without \mathcal{F}_a

We argued in the main text, that the purpose of the term \mathcal{F}_a in Equation 8 is to ensure that $\overline{w'} = \overline{a'} = 0$. It is however possible to run the MSQG model without this term (i.e., $\mathcal{F}_a = 0$). In this case, the solution converges to a different statistical equilibrium than the one we described in Section 3.2. We plot in Figure A1 the same kinetic energy figures (snapshot of kinetic energy and mean kinetic energy) that we have been plotting to do the model comparison. Although Figure A1 has a lot of common features with the reference run (Figure 2), we emphasize that this run now exhibit a mean flow $(\overline{\psi'} \neq 0)$. To highlight this mean flow, we plot in Figure A2 the upper level time mean stream function with the same contour interval as Figure 1. In this figure, we see indications that the MSQG model tends to create a large-scale flow equal and opposite to the prescribed large-scale flow. This is the case near the northern and southern boundaries. We interpret these two features as an attempt of the MSQG equation to restore a state of rest $(\psi + \Psi = 0)$. Slightly off from the western boundary, the model creates a strong northward mean flow at the central latitude which can be seen as an intensification of the western boundary current. And near the eastern boundary, we see a mean southward flow which is here harder to explain. However, since we believe the build up of this large-scale flow in the small-scale equation is spurious we do not want to comment too much this figure.

DEREMBLE ET AL. 18 of 25

19422466, 2023, 10, Downloaded from https://agupubs.onlinelibrary.wiley.com/doi/10.1029/2022MS003572 by Florida State University, Wiley Online Library on [06/06/2024]. See

on Wiley Online Library for rules of use; OA articles are governed by the applicable Creativ

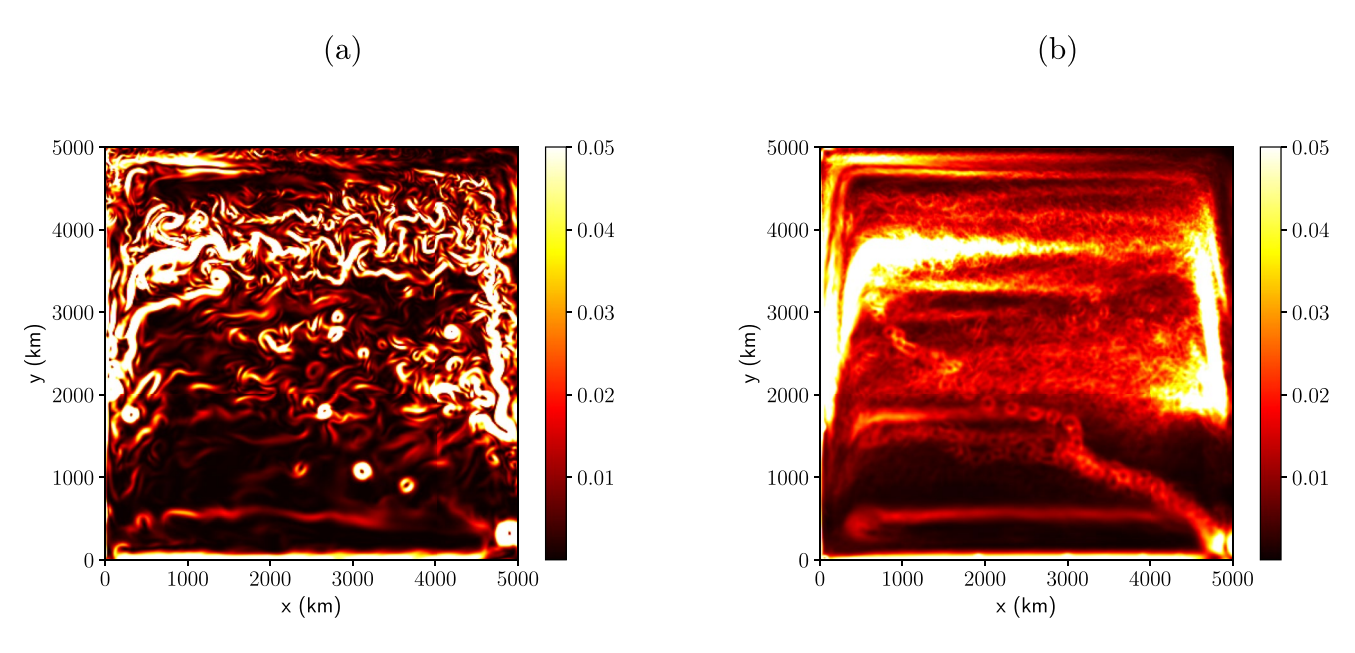


Figure A1. (a) Snapshot of kinetic energy E_k ; (b) mean kinetic energy. Both fields are in the upper level of the multiple-scale Quasi-Geostrophic model without \mathcal{F}_a (units are m² s⁻²).

A2. Traditional QG

We also briefly illustrate the type of dynamics that develop in a traditional QG model. The equations of evolution of PV are the same as the one written in this article except that the in the traditional QG, we use a uniform background stratification and uniform Coriolis parameter in the definition of PV (Equation 4). For these parameters, we take the mean values of N^2 and f over the whole domain (we still keep N^2 variable is the vertical dimension and we keep the β effect in the definition of the background PV). This really corresponds to the traditional QG equation albeit forced with a non standard background flow. Indeed we keep the same background flow that corresponds the mean velocity field of the reference model.

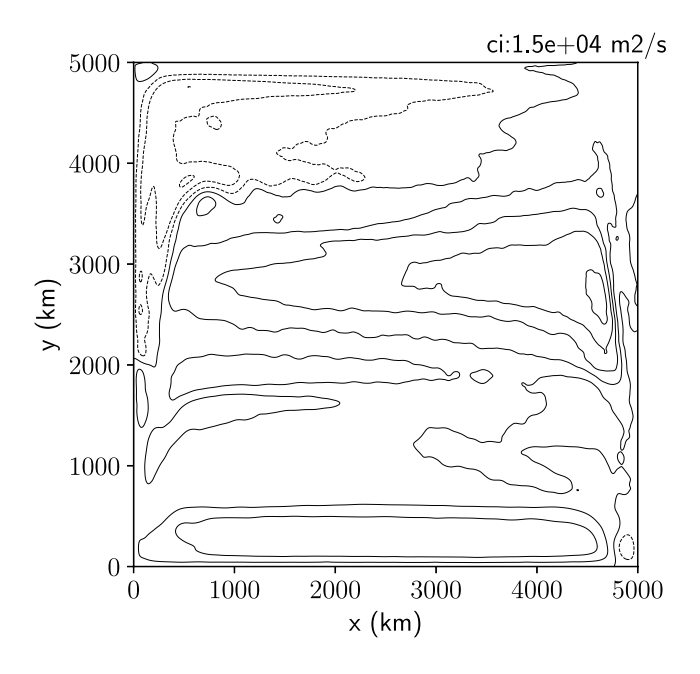


Figure A2. Mean upper level stream function of the multiple-scale Quasi-Geostrophic model without \mathcal{F}_q . Contour intervals are $1.5 \times 10^4 \,\mathrm{m^2 \, s^{-1}}$, same as Figure 1a.

DEREMBLE ET AL. 19 of 25

from https://agupubs.onlinelibrary.wiley.com/doi/10.1029/2022MS003572 by Florida State University, Wiley Online Library on [06/06/2024]. See

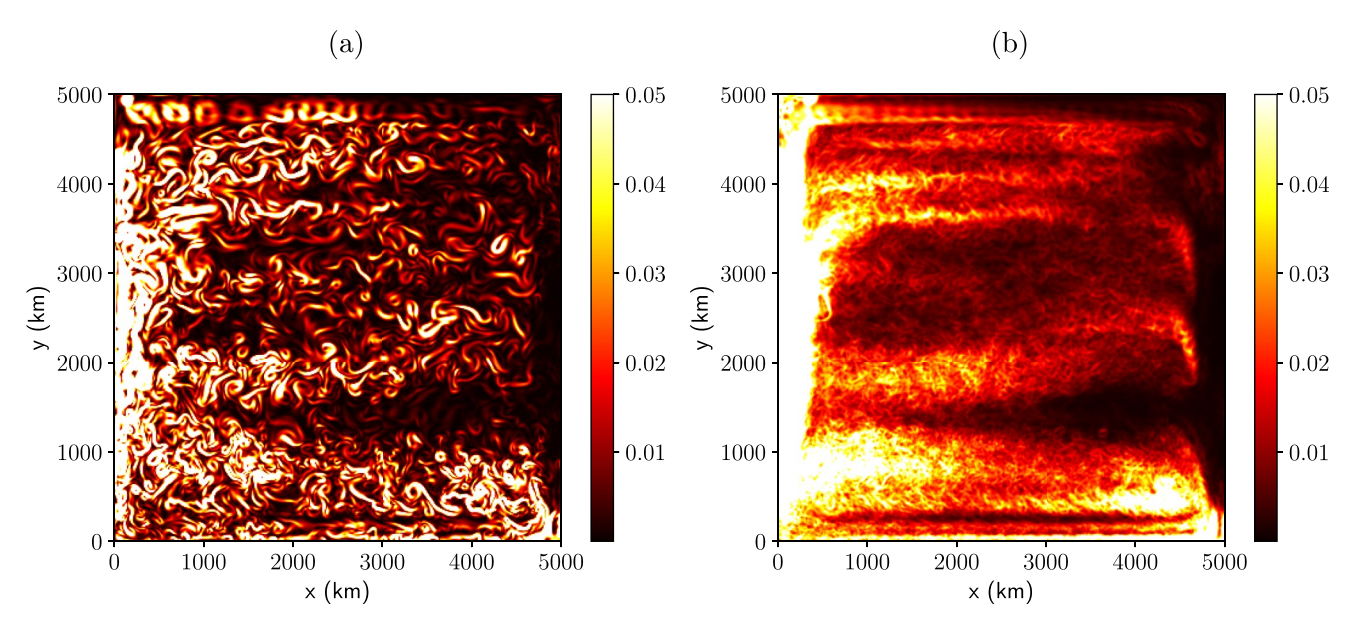


Figure A3. (a) Snapshot of kinetic energy E_k ; (b) mean kinetic energy in the upper level of the traditional Quasi-Geostrophic (QG) model. Units are $m^2 s^{-2}$ (Same as Figure 2 but for the traditional QG model).

We plot in Figure A3 a snapshot of KE and the mean KE obtained in this traditional QG model. The intensity of the eddy flow is drastically different from the reference model. This is due to the fact that for a given value of the background mean flow the stratification cannot be adjusted to tame the instability and the flow appears to be much more unstable.

Appendix B: Numerical Implementation of the MSQG Model

There are several challenges related to the numerical implementation of the multiple scale model. We present the highlights of this implementation here.

B1. Multiple Scale Derivatives

In the multiple-scale formalism, small-scale and large-scale variables are defined on two different coordinate systems which we denote (x, y) and (X, Y) respectively for this appendix only. So taking the large-scale derivative of a small-scale field (and vice versa) is zero

$$\frac{\partial u}{\partial X} = \frac{\partial U}{\partial x} = 0,\tag{B1}$$

Moreover, it is important to note that both f and N^2 are large-scale variables. In the numerical model, we make sure we do not take spurious spatial derivative of large-scale fields. For example, when we compute the gradient of the small-scale PV (for the advective term in Equation 4), we first compute the gradient of the stream function ψ and then reconstruct the gradient of the PV field, as shown here for the x derivative

$$\frac{\partial q}{\partial x} = \nabla^2 \frac{\partial \psi}{\partial x} + \Gamma \frac{\partial \psi}{\partial x}$$
 (B2a)

$$\neq \frac{\partial}{\partial x} \left(\nabla^2 \psi + \Gamma \psi \right) \tag{B2b}$$

If we use Equation B2b instead of Equation B2a, the model will exhibit a different dynamics. In fact, even the linear stability analysis reveals very different unstable modes depending on the formulation of the gradient of the large-scale PV (not shown). We recall that the correct definition of the gradient of the large-scale PV is given in Equation 12 (see also Smith, 2007).

DEREMBLE ET AL. 20 of 25

B2. Definition of the Velocity

We do one exception to the rule mentioned above for the definition of the velocity. In the original derivation of the multiple scale model, the definition of the small-scale velocity is

$$\mathbf{k} \times \mathbf{u} = -\frac{1}{f} \nabla p,\tag{B3}$$

with p the small-scale pressure. This formulation leads to several issues in the numerical formulation because (a) the velocity field is divergent, and (b) with this formulation, the model does not conserve kinetic energy (we cannot proceed with the usual integration by part because f is function of space; see below). For these two reasons, we opted for the formulation

$$\mathbf{k} \times \mathbf{u} = -\nabla \mathbf{w},\tag{B4}$$

which solves the two issues raised above. We verified that the linear instability analysis is very similar with both formulations (Equations B3 and B4) because the velocity field at each location is almost unchanged with the two formulations. Also, for the same reasons, and in order to use the same operators for the small-scale fields and the large-scale fields, we did the same simplification for definition of the large-scale velocity (see Equation 10).

B3. Vertical Discretization

An important requirement is that the large-scale stratification N^2 must be non zero to avoid a singularity in the stretching term of the QG PV. For that reason, we will implement the QG model with a small number of vertical levels (to avoid the vertical discretization of the surface mixed layer and the deep ocean). We adjust the values of N^2 to not allow any value below 10^{-6} s⁻².

We presented the QG formalism in the continuously stratified framework but once the equations are discretized in a numerical model, they are strictly equivalent to the layered equations, see (Pedlosky, 1987, Chapter 6.18). In fact, we abuse this analogy to include topographic effect and bottom drag in the model. They should normally be included as a boundary condition in the bottom buoyancy field (see Vallis, 2017, Section 5.4.3) but we instead add that boundary condition in the lower level PV dynamics as is done in the layered formalism (Hogg et al., 2003). In the lower level, the gradient of the large-scale vorticity is then

$$\overline{\nabla}Q^{l} = \left(\Gamma V + \frac{f}{h_{l}} \frac{\partial h_{b}}{\partial x}, \beta - \Gamma U + \frac{f}{h_{l}} \frac{\partial h_{b}}{\partial y}\right). \tag{B5}$$

with h_b the height of the topography and h_l the thickness of the lower layer (see Equation B.2 in Smith, 2007).

B4. Advection Operator

In traditional QG models, the numerical formulation of the advective term is usually done with the Arakawa discretization because this formulation ensures the conservation of energy and enstrophy (Cushman-Roisin & Beckers, 2011). The Arakawa Jacobian is the sum of three different discretizations $J = J^{++} + J^{+\times} + J^{\times+}$. Let us consider the advection of PV at level l which is defined as

$$q_l = \zeta_l + \Gamma_{l+1} \psi_{l+1} + \Gamma_l \psi_l + \Gamma_{l-1} \psi_{l-1} \quad \text{with} \quad \zeta_l = \nabla^2 \psi_l$$
 (B6)

We construct a numerical model of the advection operator (Equation 8) as

$$u_{l} \cdot \nabla q_{l} + U_{l} \cdot \nabla q_{l} + u_{l} \cdot \overline{\nabla} Q_{l} = J(\psi_{l}, q_{l}) + J(\Psi_{l}, q_{l}) + J(\psi_{l}, Q_{l})$$

$$= J(\psi_{l}, \zeta_{l}) + \Gamma_{l+1} J(\psi_{l}, \psi_{l+1}) + \Gamma_{l-1} J(\psi_{l}, \psi_{l-1})$$

$$+ J(\Psi_{l}, \zeta_{l}) + \Gamma_{l+1} J(\Psi_{l}, \psi_{l+1}) + \Gamma_{l-1} J(\Psi_{l}, \psi_{l-1}) + \Gamma_{l} J(\Psi_{l}, \psi_{l})$$

$$+ \Gamma_{l+1} J(\psi_{l}, \Psi_{l+1}) + \Gamma_{l-1} J(\psi_{l}, \Psi_{l-1}) + \Gamma_{l} J(\psi_{l}, \Psi_{l})$$

$$= J(\psi_{l}, \zeta_{l}) + J(\Psi_{l}, \zeta_{l})$$

$$+ \Gamma_{l+1} J(\psi_{l}, \psi_{l+1}) - \Gamma_{l-1} J(\psi_{l-1}, \psi_{l})$$

$$+ \Gamma_{l+1} J(\psi_{l}, \psi_{l+1}) - \Gamma_{l-1} J(\psi_{l-1}, \psi_{l})$$

$$+ \Gamma_{l+1} J(\psi_{l}, \Psi_{l+1}) - \Gamma_{l-1} J(\psi_{l-1}, \Psi_{l})$$

DEREMBLE ET AL. 21 of 25

Note that if we want to diagnose either $U \cdot \nabla q$, or $u \cdot \overline{\nabla} O$ individually, we then need to keep the terms $\Gamma_l J(\psi_l, \Psi_l)$ and $\Gamma_l J(\Psi_l, \psi_l)$ because they only cancel in the sum.

B5. Energy Conservation

The multi-scale model conserves energy in an asymptotic way (related to the scale separation involved in the derivation). The fact that the model does not conserve energy is not an implementation issue but is related to the derivation of the model. To illustrate this property, let us consider an isolated eddy in the middle of the ocean. We can characterize this eddy by its kinetic energy and its potential energy. If we move this eddy from one geographical location to another without deforming it, we expect that its kinetic energy remains constant. On the other hand, its potential energy is not conserved. Indeed, the potential energy of the eddy depends on its buoyancy anomaly but also of the background stratification N^2 which is a function of space. In the QG formalism, the potential energy corresponds to the APE and is defined as a small perturbation of isopycnal surfaces around reference state. If an eddy moves from one place to another, its potential energy will then vary because the reference stratification is a slow function of space.

To do an energy budget, we multiply Equation 8 by $-\psi$ and integrate over the entire domain. Let us consider only the advection of small-scale PV by the small-scale velocity

$$-\psi J(\psi, q) = -\psi J(\psi, \nabla^2 \psi + \Gamma \psi)$$

$$= -\psi J(\psi, \nabla^2 \psi) - \psi J(\psi, \Gamma \psi)$$
(B8)

The first term in the rhs is the usual kinetic energy conservation in QG, which does not pose any problem here (thanks to the non-divergent definition of the velocity). However, if we integrate the second term over the domain we have

$$\int_{\Omega} -\psi J(\psi, \Gamma \psi) = \int_{\Omega} -\frac{1}{2} J(\psi^2, \Gamma \psi)$$

$$= \int_{\Omega} \frac{1}{2} \frac{f^2}{N^2} J(\partial_z \psi^2, \partial_z \psi)$$

$$= \int_{\Omega} \frac{1}{2} \frac{f^2}{N^2} J(\psi, (\partial_z \psi)^2)$$

$$= \int_{\Omega} \frac{1}{2} \frac{f^2}{N^2} J(\psi, b^2)$$
(B9)

where we recall that we do not take derivative of the large scale variables (namely the stretching operator) and $\Gamma = \partial_z (f^2/N^2 \partial_z(\cdot))$.

The last term in the integral is formally equal to the advection of potential energy, but from a numerical prospective, this integral is non zero as soon as f^2/N^2 is non constant and so potential energy is not conserved. Again this property has a physical meaning (background stratification varies in space) and is rooted in the definition of the model. This integral vanishes in the asymptotic limit of scale separation.

There are two conditions to have a "good" energy conservation:

- Eddies should remain small compared to the horizontal variations of f and N
- f/N should remain small (which is why we imposed a minimum value on N)

As a side note, we remark that the numerical modeling community have focused a lot more on numerical schemes that conserve kinetic energy (and enstrophy) but have not really looked at potential energy conserving schemes with the notable exception of isopycnal models which conserve both mass and thus potential energy.

B6. Inversion of the Elliptic Equation

We implemented a 3D solver to invert the elliptic equation (Equation 4). We used a multigrid solver in the horizontal and solved the tridiagonal system (for the vertical stretching term) with the Thomas algorithm a each relaxation step.

DEREMBLE ET AL. 22 of 25

19422466, 2023, 10, Downloaded

Data Availability Statement

The configuration file for the MITgcm runs are available at DOI: 10.5281/zenodo.8067327 (Deremble, 2022). The source code for the multiple scale QG model is available at DOI: 10.5281/zenodo.4669909 (Deremble & Martinez, 2020).

Acknowledgments

This work is supported by NSF Grants 1434780, 1537304. TU and WKD acknowledge the support from the NSF Grant OCE-2023585, OCE-2123632, and the French "Make Our Planet Great Again" (MOPGA) program managed by the Agence Nationale de la Recherche under the Programme d'Investissement d'Avenir, reference ANR-18-MPGA-0002. Research support for RMS was provided by NASA (National Aeronautics and Space Administration) grants NNX13AD78G, NNX16AH76G and 80NSSC21K1188. We thank two anonymous reviewers for their careful reading of our manuscript and their comments. We also thank D. Balwada, P. Cessi, I. Grooms, B. Gallet and K. Julien for their insightful comments and discussions

References

- Abernathey, R., Ferreira, D., & Klocker, A. (2013). Diagnostics of isopycnal mixing in a circumpolar channel. *Ocean Modelling*, 72, 1–16. https://doi.org/10.1016/j.ocemod.2013.07.004
- Bachman, S. D. (2019). The GM+ E closure: A framework for coupling backscatter with the Gent and Mcwilliams parameterization. *Ocean Modelling*, 136, 85–106. https://doi.org/10.1016/j.ocemod.2019.02.006
- Berloff, P., Hogg, A. M., & Dewar, W. (2007). The turbulent oscillator: A mechanism of low-frequency variability of the wind-driven ocean gyres. Journal of Physical Oceanography, 37(9), 2363–2386. https://doi.org/10.1175/JPO3118.1
- Cessi, P. (2008). An energy-constrained parameterization of eddy buoyancy flux. Journal of Physical Oceanography, 38(8), 1807–1819. https://doi.org/10.1175/2007jpo3812.1
- Cessi, P., Young, W. R., & Polton, J. A. (2006). Control of large-scale heat transport by small-scale mixing. *Journal of Physical Oceanography*, 36(10), 1877–1894. https://doi.org/10.1175/JPO2947.1
- Colin de Verdiere, A. (1986). On mean flow instabilities within the planetary geostrophic equations. *Journal of Physical Oceanography*, 16(11), 1981–1984. https://doi.org/10.1175/1520-0485(1986)016(1981:OMFIWT)2.0.CO;2
- Cushman-Roisin, B., & Beckers, J.-M. (2011). Introduction to geophysical fluid dynamics: Physical and numerical aspects (Vol. 101). Academic Press.
- Deremble, B. (2022). mitgcmconfig: MITgcm configurations [Software]. https://doi.org/10.5281/zenodo.8067327
- Deremble, B., & Dewar, W. K. (2013). Volume and potential vorticity budgets of Eighteen Degree Water. *Journal of Physical Oceanography*, 43(11), 2309–2321. https://doi.org/10.1175/JPO-D-13-052.1
- Deremble, B., Johnson, E. R., & Dewar, W. K. (2017). A coupled model of interior balanced and boundary flow. *Ocean Modelling*, 119, 1–12. https://doi.org/10.1016/j.ocemod.2017.09.003
- Deremble, B., & Martinez, E. M. (2020). MSOM: Multiple scale ocean model [Software]. https://doi.org/10.5281/zenodo.4669909
- Dewar, W. K., Samelson, R. M., & Vallis, G. K. (2005). The ventilated pool: A model of subtropical mode water. *Journal of Physical Oceanog-raphy*, 35(2), 137–150. https://doi.org/10.1175/JPO-2681.1
- Eden, C., & Greatbatch, R. J. (2008). Towards a mesoscale eddy closure. Ocean Modelling, 20(3), 223–239. https://doi.org/10.1016/j.ocemod.2007.09.002
- Farrell, B. F., & Ioannou, P. J. (1999). Perturbation growth and structure in time-dependent flows. *Journal of the Atmospheric Sciences*, 56(21), 3622–3639. https://doi.org/10.1175/1520-0469(1999)056(3622:PGASIT)2.0.CO:2
- Ferrari, R., Griffies, S. M., Nurser, A. J. G., & Vallis, G. K. (2010). A boundary-value problem for the parameterized mesoscale eddy transport. Ocean Modelling, 32(3–4), 143–156. https://doi.org/10.1016/j.ocemod.2010.01.004
- Ferrari, R., McWilliams, J. C., Canuto, V. M., & Dubovikov, M. (2008). Parameterization of eddy fluxes near oceanic boundaries. *Journal of Climate*, 21(12), 2770–2789. https://doi.org/10.1175/2007jcli1510.1
- Flierl, G. R., & Pedlosky, J. (2007). The nonlinear dynamics of time-dependent subcritical baroclinic currents. *Journal of Physical Oceanogra-phy*, 37(4), 1001–1021. https://doi.org/10.1175/JPO3034.1
- Gent, P. R. (2011). The Gent–Mcwilliams parameterization: 20/20 hindsight. Ocean Modelling, 39(1–2), 2–9. https://doi.org/10.1016/j.ocemod.2010.08.002
- Gent, P. R., & McWilliams, J. C. (1990). Isopycnal mixing in ocean circulation models. *Journal of Physical Oceanography*, 20(1), 150–160. https://doi.org/10.1175/1520-0485(1990)020(0150:IMIOCM)2.0.CO;2
- Gnanadesikan, A., Pradal, M.-A., & Abernathey, R. (2015). Isopycnal mixing by mesoscale eddies significantly impacts oceanic anthropogenic carbon uptake. *Geophysical Research Letters*, 42(11), 4249–4255. https://doi.org/10.1002/2015g1064100
- Griffies, S. M. (1998). The Gent McWilliams skew flux. *Journal of Physical Oceanography*, 28(5), 831–841. https://doi. org/10.1175/1520-0485(1998)028(0831:TGMSF)2.0.CO:2
- Griffies, S. M., Winton, M., Anderson, W. G., Benson, R., Delworth, T. L., Dufour, C. O., et al. (2015). Impacts on ocean heat from transient mesoscale eddies in a hierarchy of climate models. *Journal of Climate*, 28(3), 952–977. https://doi.org/10.1175/JCLI-D-14-00353.1
- Grooms, I. (2016). A Gaussian-product stochastic Gent-Mcwilliams parameterization. Ocean Modelling, 106, 27–43. https://doi.org/10.1016/j.ocemod.2016.09.005
- Grooms, I., Julien, K., & Fox-Kemper, B. (2011). On the interactions between planetary geostrophy and mesoscale eddies. *Dynamics of Atmospheres and Oceans*, 51(3), 109–136. https://doi.org/10.1016/j.dynatmoce.2011.02.002
- Grooms, I., & Kleiber, W. (2019). Diagnosing, modeling, and testing a multiplicative stochastic Gent-Mcwilliams parameterization. *Ocean Modelling*, 133, 1–10. https://doi.org/10.1016/j.ocemod.2018.10.009
- Guillaumin, A. P., & Zanna, L. (2021). Stochastic-deep learning parameterization of ocean momentum forcing. *Journal of Advances in Modeling Earth Systems*, 13(9), e2021MS002534. https://doi.org/10.1029/2021MS002534
- $Hogg, A. M., Dewar, W. K., Killworth, P. D., \& Blundell, J. R. (2003). A quasi-geostrophic coupled model (Q-GCM). \textit{Monthly Weather Review, } 131(10), 2261-2278. \\ https://doi.org/10.1175/1520-0493(2003)131\\ \langle 2261:AQCMQ\\ \rangle 2.0.CO; 2$
- Jackson, L., Hughes, C. W., & Williams, R. G. (2006). Topographic control of basin and channel flows: The role of bottom pressure torques and friction. *Journal of Physical Oceanography*, 36(9), 1786–1805. https://doi.org/10.1175/JPO2936.1
- Jamet, Q., Deremble, B., Wienders, N., Uchida, T., & Dewar, W. (2021). On wind-driven energetics of subtropical gyres. *Journal of Advances in Modeling Earth Systems*, 13(4), e2020MS002329. https://doi.org/10.1029/2020MS002329
- Jansen, M. F., Adcroft, A., Khani, S., & Kong, H. (2019). Toward an energetically consistent, resolution aware parameterization of ocean mesoscale eddies. *Journal of Advances in Modeling Earth Systems*, 11(8), 2844–2860. https://doi.org/10.1029/2019MS001750
- Juricke, S., Danilov, S., Kutsenko, A., & Oliver, M. (2019). Ocean kinetic energy backscatter parametrizations on unstructured grids: Impact on mesoscale turbulence in a channel. *Ocean Modelling*, 138, 51–67. https://doi.org/10.1016/j.ocemod.2019.03.009
- Killworth, P. D., & Blundell, J. R. (2007). Planetary wave response to surface forcing and instability in the presence of mean flow and topography. Journal of Physical Oceanography, 37(5), 1297–1320. https://doi.org/10.1175/JPO3055.1

DEREMBLE ET AL. 23 of 25

- Li, L., Deremble, B., Lahaye, N., & Mémin, E. (2023). Stochastic data-driven parameterization of unresolved eddy effects in a baroclinic quasi-geostrophic model. *Journal of Advances in Modeling Earth Systems*, 15(2), e2022MS003297. https://doi.org/10.1029/2022MS003297
- Mak, J., Avdis, A., David, T., Lee, H. S., Na, Y., Wang, Y., & Yan, F. E. (2022). On constraining the mesoscale eddy energy dissipation time-scale. Journal of Advances in Modeling Earth Systems, 14(11), e2022MS003223. https://doi.org/10.1029/2022ms003223
- Mak, J., Marshall, D. P., Maddison, J. R., & Bachman, S. D. (2017). Emergent eddy saturation from an energy constrained eddy parameterisation. Ocean Modelline, 112, 125–138. https://doi.org/10.1016/j.ocemod.2017.02.007
- Marshall, D. P., Maddison, J. R., & Berloff, P. S. (2012). A framework for parameterizing eddy potential vorticity fluxes. *Journal of Physical Oceanography*, 42(4), 539–557. https://doi.org/10.1175/JPO-D-11-048.1
- Marshall, J., Adcroft, A., Hill, C., Perelman, L., & Heisey, C. (1997). A finite-volume, incompressible Navier Stokes model for studies of the ocean on parallel computers. *Journal of Geophysical Research*, 102(C3), 5753–5766. https://doi.org/10.1029/96JC02775
- Marshall, J., & Radko, T. (2003). Residual-mean solutions for the Antarctic circumpolar current and its associated overturning circulation. *Journal of Physical Oceanography*, 33(11), 2341–2354. https://doi.org/10.1175/1520-0485(2003)033(2341:RSFTAC)2.0.CO;2
- McDougall, T. J., & McIntosh, P. C. (2001). The temporal-residual-mean velocity. Part II: Isopycnal interpretation and the tracer and momentum equations. *Journal of Physical Oceanography*, 31(5), 1222–1246. https://doi.org/10.1175/1520-0485(2001)031<1222:ttrmvp>2.0.co;2
- Mémin, E. (2014). Fluid flow dynamics under location uncertainty. Geophysical & Astrophysical Fluid Dynamics, 108(2), 119–146. https://doi.org/10.1080/03091929.2013.836190
- Meunier, J., Miquel, B., & Gallet, B. (2023). A direct derivation of the Gent–Mcwilliams/Redi diffusion tensor from quasi-geostrophic dynamics. Journal of Fluid Mechanics. 963, A22, https://doi.org/10.1017/ifm.2023.347
- Nakamura, M., & Chao, Y. (2000). On the eddy isopycnal thickness diffusivity of the Gent-Mcwilliams subgrid mixing parameterization. *Journal of Climate*, 13(2), 502–510. https://doi.org/10.1175/1520-0442(2000)013(0502:OTEITD)2.0.CO;2
- Nikurashin, M., & Vallis, G. K. (2012). A theory of the interhemispheric meridional overturning circulation and associated stratification. *Journal of Physical Oceanography*, 42(10), 1652–1667. https://doi.org/10.1175/JPO-D-11-0189.1
- Pedlosky, J. (1984). The equations for geostrophic motion in the ocean. *Journal of Physical Oceanography*, 14(2), 448–456. https://doi.org/10.1 175/1520-0485(1984)014(0448:TEFGMI)2.0.CO:2
- Pedlosky, J. (1987). Geophysical fluid dynamics (2nd ed., p. 636). Springer-Verlag. 1982.
- Porta Mana, P., & Zanna, L. (2014). Toward a stochastic parameterization of ocean mesoscale eddies. Ocean Modelling, 79, 1–20. https://doi.org/10.1016/j.ocemod.2014.04.002
- Rhines, P. B., & Young, W. R. (1982). Homogenization of potential vorticity in planetary gyres. *Journal of Fluid Mechanics*, 122(-1), 347–367. https://doi.org/10.1017/S0022112082002250
- Roullet, G., McWilliams, J. C., Capet, X., & Molemaker, M. J. (2012). Properties of steady geostrophic turbulence with isopycnal outcropping. *Journal of Physical Oceanography*, 42(1), 18–38. https://doi.org/10.1175/JPO-D-11-09.1
- Ryzhov, E. A., Kondrashov, D., Agarwal, N., McWilliams, J. C., & Berloff, P. (2020). On data-driven induction of the low-frequency variability in a coarse-resolution ocean model. *Ocean Modelling*, 153, 101664. https://doi.org/10.1016/j.ocemod.2020.101664
- Salmon, R. (1994). Generalized two-layer models of ocean circulation. Journal of Marine Research, 52(5), 865–908. https://doi.org/10.1357/0022240943076939
- Samelson, R. M., Chelton, D. B., & Schlax, M. G. (2019). The ocean mesoscale regime of the reduced-gravity quasigeostrophic model. *Journal of Physical Oceanography*, 49(10), 2469–2498. https://doi.org/10.1175/JPO-D-18-0260.1
- Samelson, R. M., & Vallis, G. K. (1997a). A simple friction and diffusion scheme for planetary geostrophic basin models. *Journal of Physical Oceanography*, 27(1), 186–194. https://doi.org/10.1175/1520-0485(1997)027/0186;ASFADS)2.0.CO;2
- Samelson, R. M., & Vallis, G. K. (1997b). Large-scale circulation with small diapycnal diffusion: The two-thermocline limit. *Journal of Marine Research*, 55(2), 223–275. https://doi.org/10.1357/0022240973224382
- Shevchenko, I. V., & Berloff, P. S. (2015). Multi-layer quasi-geostrophic ocean dynamics in eddy-resolving regimes. Ocean Modelling, 94, 1–14. https://doi.org/10.1016/j.ocemod.2015.07.018
- Simonnet, E., Rolland, J., & Bouchet, F. (2021). Multistability and rare spontaneous transitions in barotropic beta-plane turbulence. *Journal of the Atmospheric Sciences*, 78(6), 1889–1911. https://doi.org/10.1175/JAS-D-20-0279.1
- Smith, K. (2007). The geography of linear baroclinic instability in earth's oceans. Journal of Marine Research, 65(5), 655–683. https://doi.org/10.1357/002224007783649484
- Stewart, A. L., McWilliams, J. C., & Solodoch, A. (2021). On the role of bottom pressure torques in wind-driven gyres. *Journal of Physical Oceanography*, 51(5), 1441–1464. https://doi.org/10.1175/JPO-D-20-0147.1
- Theiss, J. (2006). A generalized Rhines effect and storms on Jupiter. Geophysical Research Letters, 33(8), L08809. https://doi.org/10.1029/2005GL025379
- Toggweiler, J. R., & Samuels, B. (1995). Effect of Drake Passage on the global thermohaline circulation. *Deep Sea Research Part 1: Oceano-graphic Research Papers*, 42(4), 477–500. https://doi.org/10.1016/0967-0637(95)00012-U
- Treguier, A. M., Held, I. M., & Larichev, V. D. (1997). Parameterization of quasigeostrophic eddies in primitive equation ocean models. *Journal of Physical Oceanography*, 27(4), 567–580. https://doi.org/10.1175/1520-0485(1997)027(0567:POQEIP)2.0.CO;2
- Tulloch, R., Marshall, J., Hill, C., & Smith, K. S. (2011). Scales, growth rates, and spectral fluxes of baroclinic instability in the ocean. *Journal of Physical Oceanography*, 41(6), 1057–1076. https://doi.org/10.1175/2011JPO4404.1
- Uchida, T. (2019). Seasonality in surface (sub) mesoscale turbulence and its impact on iron transport and primary production (Doctoral dissertation). Columbia University in the City of New York. https://doi.org/10.7916/d8-9s8r-m049
- Uchida, T., Balwada, D., Jamet, Q., Dewar, W., Deremble, B., Penduff, T., & Le Sommer, J. (2023). Cautionary tales from the mesoscale eddy diffusivity tensor. *Ocean Modelling*, 182, 102172. https://doi.org/10.1016/j.ocemod.2023.102172
- Uchida, T., Deremble, B., & Penduff, T. (2021). The seasonal variability of the ocean energy cycle from a quasi-geostrophic double gyre ensemble. Fluids, 6(6), 206. https://doi.org/10.3390/fluids6060206
- Uchida, T., Deremble, B., & Popinet, S. (2022). Deterministic model of the eddy dynamics for a midlatitude ocean model. *Journal of Physical Oceanography*, 52(6), 1133–1154. https://doi.org/10.1175/JPO-D-21-0217.1
- Vallis, G. K. (2017). Atmospheric and oceanic fluid dynamics: Fundamentals and large-scale circulation (2nd ed.). Cambridge University Press.
 Venaille, A., Vallis, G. K., & Smith, K. S. (2011). Baroclinic turbulence in the ocean: Analysis with primitive equation and quasigeostrophic simulations. Journal of Physical Oceanography, 41(9), 1605–1623. https://doi.org/10.1175/JPO-D-10-05021.1
- Visbeck, M., Marshall, J., Haine, T., & Spall, M. (1997). Specification of eddy transfer coefficients in coarse-resolution ocean circulation models. *Journal of Physical Oceanography*, 27(3), 381–402. https://doi.org/10.1175/1520-0485(1997)027<0381:soetci>2.0.co;2
- Warren, B. A. (1990). Suppression of deep oxygen concentrations by Drake Passage. Deep Sea Research Part 1: Oceanographic Research Papers, 37(12), 1899–1907. https://doi.org/10.1016/0198-0149(90)90085-A

DEREMBLE ET AL. 24 of 25



Journal of Advances in Modeling Earth Systems

10.1029/2022MS003572

Waterman, S., & Jayne, S. R. (2011). Eddy-mean flow interactions in the along-stream development of a western boundary current jet: An idealized model study. *Journal of Physical Oceanography*, 41(4), 682–707. https://doi.org/10.1175/2010JPO4477.1

Wunsch, C., & Ferrari, R. (2004). Vertical mixing, energy, and the general circulation of the oceans. *Annual Review of Fluid Mechanics*, 36(1), 281–314. https://doi.org/10.1146/annurev.fluid.36.050802.122121

Zhao, R., & Vallis, G. (2008). Parameterizing mesoscale eddies with residual and Eulerian schemes, and a comparison with eddy-permitting models. *Ocean Modelling*, 23(1–2), 1–12. https://doi.org/10.1016/j.ocemod.2008.02.005

DEREMBLE ET AL. 25 of 25